JUL 08 2002 0830-L-02 NAS 1.29/3-2:02-05

NASA TechBriefs

National Aeronautics and
Space Administration

Electronic Components and Circuits

Electronic Systems

Physical Sciences

Materials

Computer Programs

Mechanics

Machinery

Fabrication Technology

Mathematics and Information Sciences

Life Sciences

02-05

May 2002

2002-02748 MH C

INTRODUCTION

Tech Briefs are short announcements of innovations originating from research and development activities of the National Aeronautics and Space Administration. They emphasize information considered likely to be transferable across industrial, regional, or disciplinary lines and are issued to encourage commercial application.

Availability of NASA Tech Briefs and TSPs

Requests for individual Tech Briefs or for Technical Support Packages (TSPs) announced herein should be addressed to

National Technology Transfer Center
Telephone No. **(800) 678-6882** or via World Wide Web at **www2.nttc.edu/leads/**

Please reference the control numbers appearing at the end of each Tech Brief. Information on NASA's Commercial Technology Team, its documents, and services is also available at the same facility or on the World Wide Web at **www.nctn.hq.nasa.gov**.

Commercial Technology Offices and Patent Counsels are located at NASA field centers to provide technology-transfer access to industrial users. Inquiries can be made by contacting NASA field centers and program offices listed below.

NASA Field Centers and Program Offices

Ames Research Center
Carolina Blake
(650) 604-1754 or
cblake@mail.arc.nasa.gov

Dryden Flight Research Center
Jenny Baer-Riedhart
(661) 276-3689 or
jenny.baer-riedhart@dfrc.nasa.gov

Goddard Space Flight Center
George Alcorn
(301) 286-5810 or
galcorn@gsfc.nasa.gov

Jet Propulsion Laboratory
Merle McKenzie
(818) 354-2577 or
merle.mckenzie@jpl.nasa.gov

Johnson Space Center
Hank Davis
(281) 483-0474 or
henry.l.davis1@jsc.nasa.gov

John F. Kennedy Space Center
Jim Aliberti
(321) 867-6224 or
Jim.Aliberti-1@ksc.nasa.gov

Langley Research Center
Sam Morello
(757) 864-6005 or
s.a.morello@larc.nasa.gov

Glenn Research Center
Larry Viterna
(216) 433-3484 or
cto@grc.nasa.gov

George C. Marshall Space Flight Center
Vernotto C. McMillan
(256) 544-2615 or
vernotto.mcmillan@msfc.nasa.gov

John C. Stennis Space Center
Kirk Sharp
(228) 688-1929 or
technology@ssc.nasa.gov

NASA Program Offices
At NASA Headquarters there are seven major program offices that develop and oversee technology projects of potential interest to industry:

Carl Ray
Small Business Innovation Research Program (SBIR) & Small Business Technology Transfer Program (STTR)
(202) 358-4652 or
cray@mail.hq.nasa.gov

Dr. Robert Norwood
Office of Commercial Technology (Code RW)
(202) 358-2320 or
rnorwood@mail.hq.nasa.gov

John Mankins
Office of Space Flight (Code MP)
(202) 358-4659 or
jmankins@mail.hq.nasa.gov

Terry Hertz
Office of Aero-Space Technology (Code RS)
(202) 358-4636 or
thertz@mail.hq.nasa.gov

Glen Mucklow
Office of Space Sciences (Code SM)
(202) 358-2235 or
gmucklow@mail.hq.nasa.gov

Roger Crouch
Office of Microgravity Science Applications (Code U)
(202) 358-0689 or
rcrouch@hq.nasa.gov

Granville Paules
Office of Mission to Planet Earth (Code Y)
(202) 358-0706 or
gpaules@mtpe.hq.nasa.gov

BLANK PAGE

NASA TechBriefs

National Aeronautics and
Space Administration

May 2002
02-05

5 Electronic Components and Circuits

11 Electronic Systems

15 Physical Sciences

23 Materials

31 Computer Programs

35 Mechanics

41 Machinery

45 Fabrication Technology

49 Mathematics and Information Sciences

This document was prepared under the sponsorship of the National Aeronautics and Space Administration. Neither the United States Government nor any person acting on behalf of the United States Government assumes any liability resulting from the use of the information contained in this document, or warrants that such use will be free from privately owned rights.

BLANK PAGE

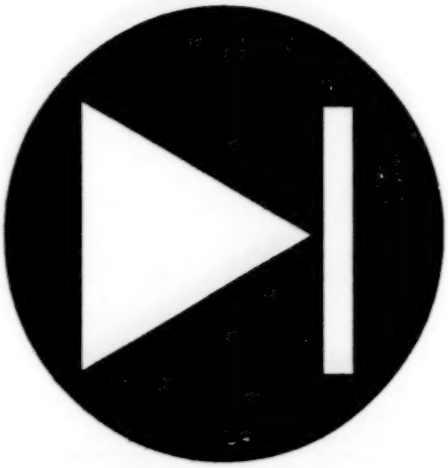

Electronic Components and Circuits

Hardware, Techniques, and Processes

7 Circuits Control Test Power-Turn-On and -Turn-Off Transients
7 Arrays of QWIPs With Spatial Separation of Multiple Colors
8 Multiple-Cavity Masers as 32-GHz LNAs

Books and Reports

9 Study of Amplification in Optocoupler-Equivalent Circuits

BLANK PAGE

Circuits Control Test Power-Turn-On and -Turn-Off Transients

Transients are repeatable and can be timed or phased precisely.

Marshall Space Flight Center, Alabama

Two electronic circuits that generate controlled power-turn-on and power-turn-off transients have been developed. These circuits are parts of a suite of test equipment used to measure the responses, to power-bus transients, of power supplies and power-consuming electronic circuitry aboard the space shuttle. These circuits can also be used in testing responses to power-bus transients in other closed electronic systems that include power sources and power-consuming equipment.

The figure is a simplified block diagram of the relationships among these circuits, a power source, and a piece of equipment under test (EUT). The power-distribution wiring between the power source and the EUT is modeled by a line impedance stabilization network (LISN), which is a circuit that contains lumped resistance(s), capacitance(s), and/or inductance(s). One of the circuits, called a "precision phase-controlled power switch" ("emission switch" for short), is designed specifically for turning on and/or turning off the power supplied to the EUT. The other circuit, called a "switching transient simulator" ("STS" for short), injects transients from a switched resistor-and-capacitor load into the connection between the LISN and the EUT to simulate the switching of power to circuits other than the EUT.

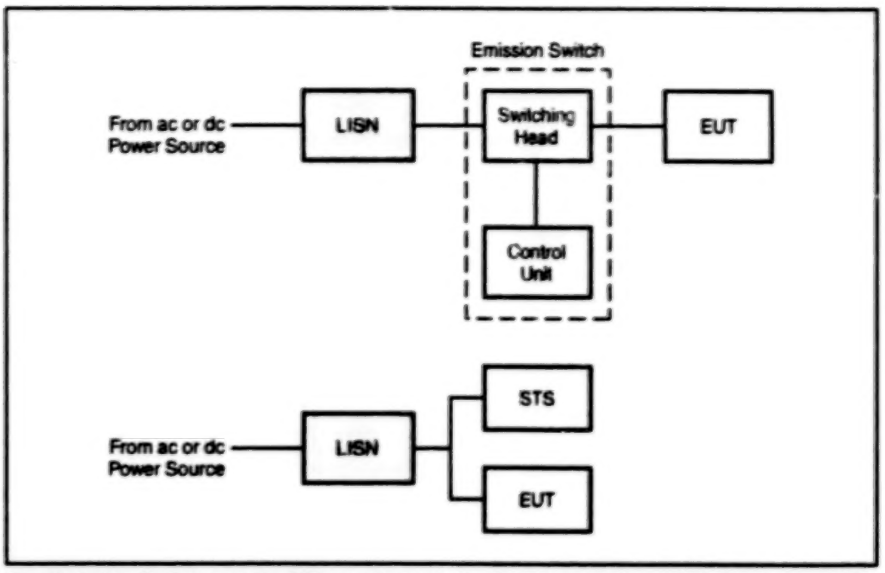

The Emission Switch and the STS are electronic circuits that generate precisely timed, repeatable switching transients for testing the EUT.

Prior to the development of the emission switch and the STS, turn-on and turn-off transients for testing were generated by use of mechanical switches. One disadvantage of mechanical switches is that they are susceptible to contact bounce and arcing, which give rise to nonreapeatability of switching waveforms. Another disadvantage of mechanical switches is that their opening and closing times cannot be controlled precisely; this is especially important in the case of an ac power supply, inasmuch as the open-switch voltage an infinitesimal time before turn-on or the closed-switch current an infinitesimal time before turn-off depends on the phase (that is, the time from the beginning of the power-supply cycle).

In the emission switch and the STS, the primary switching elements are field-effect transistors (FETs), which, unlike mechanical switches, are not susceptible to bounce or arcing. Moreover, FETs can be turned on or off starting at precise instants of time and with repeatable rise or fall times, by use of control signals with suitably timed and shaped waveforms. Both the emission switch and the STS can be synchronized with an ac power waveform so that they generate the required "on" or "off" transients at specified phases of the power cycle.

An additional notable feature of the emission switch is the inclusion of a timed mechanical relay switch. This switch is turned on 10 ms after the FET has been turned on and is turned off 10 ms before the FET is turned off. Thus, except for 10-ms intervals at the beginning and end of the "on" time, the mechanical switch bypasses the FET. This feature reduces the time-averaged power dissipated in the FET, thereby reducing the FET heat-sinking requirement.

This work was done by Ken Javor of EMC Compliance for **Marshall Space Flight Center**. *Further information is contained in a TSP [see page 1].*

MFS-31457

Arrays of QWIPs With Spatial Separation of Multiple Colors

Spectral imagers could be made simpler, smaller, lighter, and less costly.

NASA's Jet Propulsion Laboratory, Pasadena, California

Focal-plane arrays of quantum-well infrared photodetectors (QWIPs) featuring adjacent pixels sensitive to different colors have been proposed. An array of this type would make it possible to image the same scene in multiple wavelength bands simultaneously on the same focal plane, without need for moving parts or for complex optics to split light into wavelength bands and make the light in each band impinge on a separate detector array optimized for that band. Hence, these arrays would make it possible to develop a new generation of spectral imagers that would be smaller, lighter, and less costly, relative to spectral imagers now or previously in use.

The figure is a schematic cross section of one pixel of a four-color array according to the proposal. The pixel would be divided into four adjacent sub-pixels, each sub-pixel optimized for one of the four desired wavelength bands. All the sub-pixels would contain identical stacks of four multiple-quantum-well (MQW) photodetectors (for all four bands), but as described below, functional electrical connections would be made to only the one MQW photodetector that was optimized for the wavelength band assigned to a given sub-pixel.

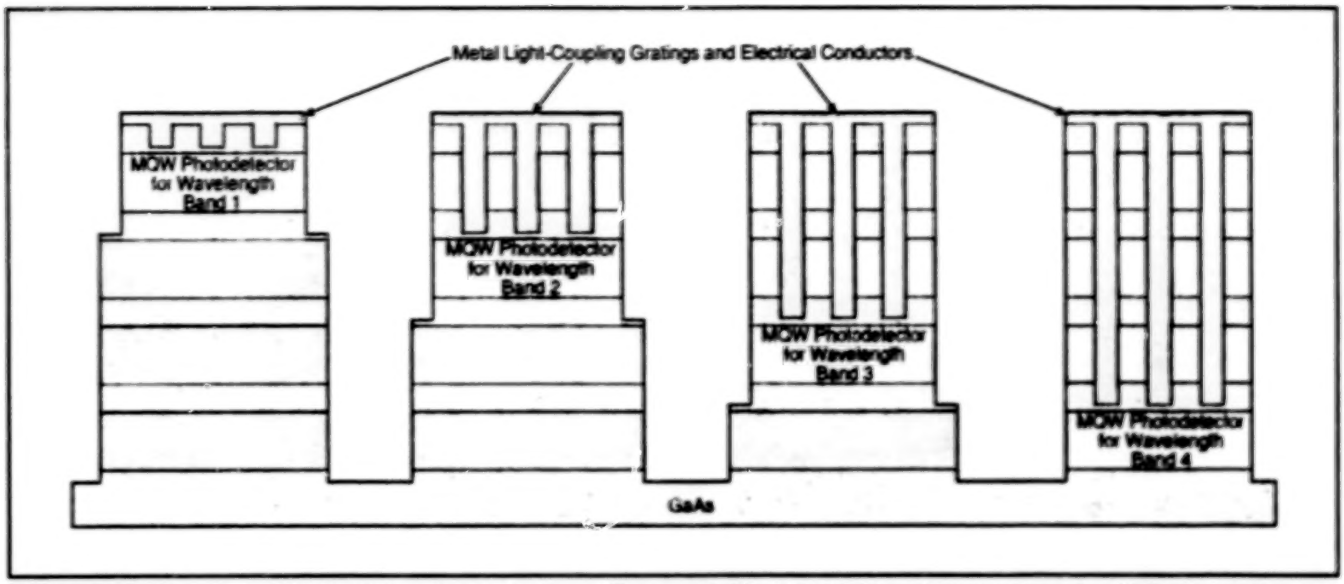
Metal Light-Coupling Gratings and Electrical Conductors
MQW Photodetector for Wavelength Band 1
MQW Photodetector for Wavelength Band 2
MQW Photodetector for Wavelength Band 3
MQW Photodetector for Wavelength Band 4
GaAs

Sub-Pixel Stacks would contain identical semiconductor layers. They would differ in their light-coupling two-dimensional diffraction gratings and electrical contacts.

Each MQW photodetector in a stack would comprise 30 spatial periods of layers of GaAs quantum wells separated by $Al_xGa_{1-x}As$ barriers; the parameters of the layers would be chosen to maximize sensitivity in the designated wavelength bands. The photodetectors for the different wavelength bands would be separated by intermediate contact layers.

Fabrication of the array would begin with the growth of a wafer comprising all of the MQW, contact, and ancillary GaAs and $Al_xGa_{1-x}As$ semiconductor layers. Next, the pixels and sub-pixels would be defined by photolithographic processing, including masking, etching, chemical vapor deposition, and deposition of metal. The wavelength band for each sub-pixel stack would be delineated by use of a deep groove etch to make contact with the intermediate contact layers of the MQW photodetector for that band while short-circuiting the contact layers of the MQW photodetectors for the other bands. Short-circuiting would be effected by forming grids of gold-coated, reflective etched lines. In addition to serving as shorting conductors, these grids would constitute two-dimensional diffraction gratings that would be optimized for coupling light into the MQWs. For multicolor QWIPs, the grating grooves also serve to deactivate redundant quantum-well stacks (see figure). To ensure sufficient groove depth to penetrate inactive quantum-well stacks, as well as to provide light coupling, three-quarter or five-quarter wavelength groove depths have been used. [The need for such light couplers and the use of two-dimensional diffraction gratings to satisfy this need was described in "Cross-Grating Coupling for Focal-Plane Arrays of QWIPs" (NPO-19657), *NASA Tech Briefs*, January 1998.]

This work was done by Sumith Bandara, Sarath Gunapala, John K. Liu, David Ting, Sir B. Rafol, and Jason Mumolo of Caltech for **NASA's Jet Propulsion Laboratory.** *Further information is contained in a TSP [see page 1].*

In accordance with Public Law 96-517, the contractor has elected to retain title to this invention. Inquiries concerning rights for its commercial use should be addressed to

Intellectual Property group
JPL
Mail Stop 202-233
4800 Oak Grove Drive
Pasadena, CA 91109
(818) 354-2240

Refer to NPO-21084, volume and number of this NASA Tech Briefs issue, and the page number.

Multiple-Cavity Masers as 32-GHz LNAs

Advanced designs feature compactness and high performance.

NASA's Jet Propulsion Laboratory, Pasadena, California

Improved multiple-cavity ruby masers are under development for use as low-noise amplifiers (LNAs) for receiving very weak radio signals in frequency bands up to and including one centered approximately at 32 GHz. These masers were designed specifically to be incorporated into receivers in ground stations of NASA's Deep Space Network. The design may be useful in terrestrial cellular telephone terminals where high selectivity and immunity to the generation of intermodulation products may be needed.

The designs simplify field operations, afford high reliability, minimize required pump power levels, and provide noise temperatures near quantum limits. The low pump-power requirements enable operation in commercially available closed-cycle helium refrigerators at temperatures of ≤4 K. Another important aspect of the designs is small size, enabling the placement of many amplifiers in a single refrigerator in support of arrayed feeds, operation at multiple frequencies, and/or simultaneous dual-polarization operation, some or all of which are needed in many receiving systems.

A maser of this type includes a ruby-filled cavity, one or more signal-coupling cavities, one or more pump-coupling cavities, and a pump-reject filter, all combined in a single amplifier assembly. Signals are routed to and from the amplifier assembly via a transmission line (which is a waveguide in the case of 32 GHz) connected to a circulator. At 32 GHz, the amplifiers are small enough that twelve of them can fit within a single solenoid that has an inner diameter of 10 cm.

Each amplifying cavity is a half-wavelength waveguide resonator filled with ruby (having dimensions of 2.601 by 1.3005 by 1.016 mm in the 32-GHz case). The pump-reject filter is located in a waveguide, called the "signal waveguide," between the ruby and the circulator. This filter reflects the pump energy that has passed through the ruby back to the ruby, thereby confining the pump energy to the amplifier in order to maximize the pumping efficiency.

The tuning range of the 32-GHz version covers the deep-space-to-Earth frequency allocation of 31.8 GHz to 32.3 GHz with an instantaneous bandwidth of at least 100 MHz and an amplifier noise temperature of 3.1 K. Slightly lower noise temperature may be possible when this maser is operated in a refrigerator at a physical temperature <2.2 K.

This work was done by James Shell and Robert Clauss of Caltech for **NASA's Jet Propulsion Laboratory**. *Further information is contained in a TSP [see page 1].*

In accordance with Public Law 96-517, the contractor has elected to retain title to this invention. Inquiries concerning rights for its commercial use should be addressed to

Intellectual Property group
JPL
Mail Stop 202-233
4800 Oak Grove Drive
Pasadena, CA 91109
(818) 354-2240

Refer to NPO-30143, volume and number of this NASA Tech Briefs *issue, and the page number.*

Books and Reports

Study of Amplification in Optocoupler-Equivalent Circuits

A report presents a theoretical and experimental study of amplification in electronic circuits that include combinations of discrete light sources (e.g., light-emitting diodes) and photodetectors (e.g., reverse-biased photodiodes), which combinations perform essentially the same functions as do the commercially available, packaged light-source/photodetector combinations denoted, variously, as optocouplers, optoisolators, and the like. The report calls these circuits photo-electric amplifiers (which should not be confused with photoelectric amplifiers). The report discusses the basic considerations of current, voltage, impedance, transformer coupling, source/detector optical coupling, bias and load resistances, and other phenomena that affect current, voltage, and power gains. Limitations and design concerns for making photo-electric amplifiers function as linear amplifiers are also discussed. Tests of amplifiers and oscillators based on photo-electric amplifiers are described. An addendum to the report discusses the use of photo-electric amplifiers to make digital-logic elements for data-processing circuits ranging from process controllers to computers. Finally, it is reported that experimental AND, OR, and NOT gates were constructed and tested to demonstrate this concept and were found to function as predicted.

This work was done by John M. Franke of **Langley Research Center**. *To obtain a copy of the report, "Photo-Electric Amplifier," see TSP's [page 1].*
LAR-15460

BLANK PAGE

Electronic Systems

Hardware, Techniques, and Processes

13 Stabilization and Registration of Sequential Video Images

13 Loss-Tolerant Speech Codec

BLANK PAGE

Stabilization and Registration of Sequential Video Images

Images are corrected for translation, rotation, and dilation.

Marshall Space Flight Center, Alabama

A computational process converts a sequence of digitized video images of the same scene into stabilized, coregistered images of an area of interest within the scene. The process corrects for motion of the area of interest or of the camera (as manifested by rotation, translation, and/or dilation of the raw images). Thus, there is minimal translation, rotation, or dilation in the sequence of output images of the area of interest. The stabilization and coregistration of images can facilitate scientific, engineering, or forensic analysis of the area of interest. Alternatively or in addition, the output images can be used to synthesize a single video image with reduced noise.

Older processes that were developed to serve the same purpose correct for translation but not for rotation or dilation. They are sensitive to effects of parallax (as manifested in differences between velocities of foreground and background objects). Most of them are not capable of resolving image displacements to resolutions finer than one pixel. The present process not only corrects for both rotation and dilation but is also less sensitive to parallax and can resolve motion and achieve registration to within a fraction of a pixel.

The process begins with the selection of an initial or reference video field — the key field — that includes the area of interest. The other fields in the sequence are known as test fields. The area of interest in the key field is identified and extracted for comparison with a corresponding area of the same size in each test field. Cross-correlations between the area-of-interest subimages of the key and test field are computed, and the translational offset (comprising horizontal and vertical displacements) between these subimages is estimated by selecting that offset that maximizes the correlation coefficient.

The areas of interest in the key and test fields are subdivided into blocks of pixels, for which cross-correlations are computed and offsets are estimated, using the previously estimated offset as initial estimates. The blocks are then further subdivided for computation of cross-correlations and offsets. The procedure of subdivision, cross-correlation, and offset estimation is repeated several times, yielding a hierarchy of block sizes (typically, down to smallest block size of 10 by 10 pixels) with corresponding correlation coefficients and offsets.

A data mask is constructed for the offsets at each level of the hierarchy to exclude those offsets that are deemed to be questionable because their correlation coefficients are below an arbitrary threshold value. The final offsets for the test field are calculated as weighted averages of the unmasked offsets for all block sizes; the weights are proportional to the sizes of the blocks. The data mask and the multiplicity of data from different parts of the area of interest help to reduce errors caused by parallax.

The rotation and dilation of the test field relative to the key field are estimated from the curls and divergences, respectively, of unmasked offset vectors. Statistical outliers (beyond one standard deviation) of curl and divergence values are masked out. The final offsets, rotation, and dilation are used to transform the test field into an output field that matches the key field in position, orientation, and magnification. The entire process is then repeated for each subsequent test field, using the offsets from the preceding field as initial guesses to reduce the ranges of offsets that must be searched for maximum correlation coefficients.

This work was done by David H. Hathaway and Paul J. Meyer of **Marshall Space Flight Center**.

This invention is owned by NASA, and a patent application has been filed. Inquiries concerning nonexclusive or exclusive license for its commercial development should be addressed to Sammy Nabors, MSFC Commercialization Assistance Lead, at (256) 544-5226 or sammy.nabors@msfc.nasa.gov. Refer to MFS-31243.

Loss-Tolerant Speech Codec

The design is based on the dynamics of speech, which can be learned off-line.

Lyndon B. Johnson Space Center, Houston, Texas

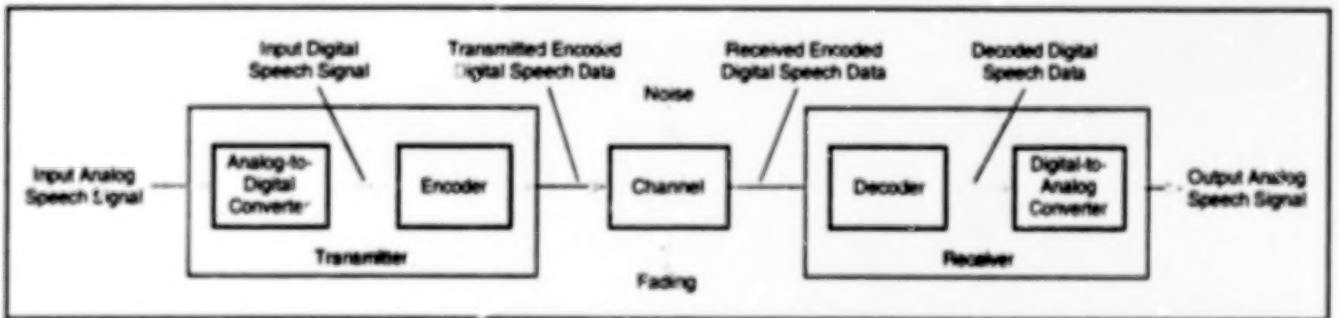

The Decoder in the Loss-Tolerant Speech Codec estimates speech represented by missing or erroneous frames of received speech data. The estimate is an extrapolation based on the data from preceding frames and on the dynamics of speech as learned by a back-propagation neural network.

A coder/decoder system (codec) is being developed for use in a digital voice communication system in which speech is encoded as a series of frames of data and transmitted over a noisy or lossy channel. Called a "loss-tolerant speech codec" (LTSC), the system is designed to maintain the quality of reconstructed speech at the receiver (decoder) when frames are occasionally lost or corrupted by noise during propagation through the channel. Digital satellite and digital cellular telephone links are typical examples of channels in which frames can be lost or corrupted by noise. In addition, variable frame delays in packet-switching digital communication channels can occasionally become long enough to exert the same effect upon

speech decoders as that of loss of speech during the affected frames.

The principal innovative aspect of this LTSC is a subsystem called an "intelligent speech filter" (ISF), which combines the latest neural-network technology with state-of-the-art speech-processing techniques. The ISF functions as a speech predictor or extrapolator; it reconstructs an approximate version of the missing speech frames on the basis of previous speech frames and of its knowledge of the dynamics of the vocal tract and pitch. The quality of speech reconstructed after transmission through a noisy channel is improved over that of other codecs because in a dynamical sense, the estimated speech inserted in the missing or erroneous frames sounds like the immediately preceding speech. In contrast, other codecs put out such distracting, discontinuous sounds as clicks, abrupt silences, or garbled speech in response to missing or erroneous frames.

The design of this LTSC will eventually call for high-speed microprocessors, parallel processing architecture, and efficient algorithm coding to implement its functions, which are shown in simplified form in the figure. The analog-to-digital converter in the transmitter linearly quantizes the input speech signal into a binary representation of 12 to 16 bits at a sampling rate of f_s. The digital input speech signal estimates the spectral envelope that represents the vocal tract, along with an appropriate driving function. Within the encoder, the digital input speech signal is first classified as either voiced or unvoiced, because the mathematical models for processing voiced and unvoiced signals are quite different; the model for voiced signals involves pitch-synchronous spectral analysis, while that for unvoiced signals involves linear prediction spectral analysis.

The decoder in the receiver includes the ISF plus signal-processing circuitry that determines whether or not each received frame of data is erroneous. If a frame is received without error, the data are decoded into a spectral envelope, frame energy, and pitch period for voiced speech. The decoded data are used to generate a speech time series, which is fed to a digital-to-analog converter for conversion to an analog output speech signal.

The decoded data are also sent to an input buffer in the ISF. When a frame of data is found to be lost or erroneous, the ISF uses the decoded data stored in the buffer during preceding frames to extrapolate the spectral envelope, energy, and pitch period into the missing or erroneous frame. The energy and pitch are both predicted by an all-pole infinite-impulse-response digital filter. The neural network is used to solve the most difficult part of the extrapolation problem, which is prediction of the spectral envelope.

The neural network is of a back-propagation-learning type. The neural network can be trained in the dynamics of speech by use of the time-varying spectral envelopes of representative samples of speech recorded from a variety of speakers. The neural network in the prototype ISF was trained on a single sentence from a single speaker, but the training set will eventually be expanded to include many sentences from many speakers, containing all phonemes and phoneme transitions.

This work was done by Jaime L. Prieto of LinCom Corp. for **Johnson Space Center**. *No further documentation is available.*

In accordance with Public Law 96-517, the contractor has elected to retain title to this invention. Inquiries concerning rights for its commercial use should be addressed to

Jaime L. Prieto
LinCom Corp.
1020 Bay Area Blvd.
Suite 200
Houston, TX 77058

Refer to MSC-22426, volume and number of this NASA Tech Briefs *issue, and the page number.*

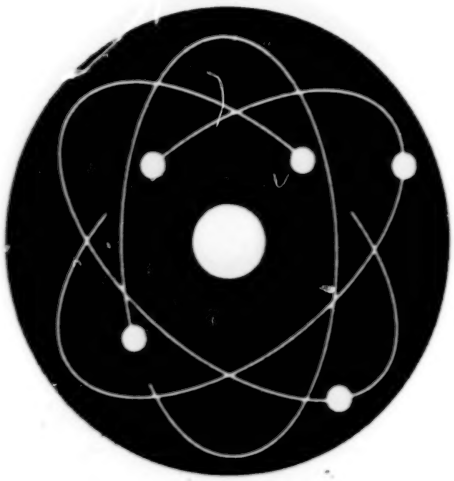

Physical Sciences

Hardware, Techniques, and Processes

17 Characterization of Heat-Flux-Gauge Calibration System
18 Two-Fiber-Optic Method of Laser Doppler Velocimetry
19 Software for Electromagnetic Detection of Buried Explosives
19 Aircraft Anti-Icing Systems Utilizing Induced Hydrophobicity

Books and Reports

20 Paraffin-Actuated Heat Switch for Mars Surface Applications
20 Inhibited Carrier Transfer in Ensembles of Quantum Dots
21 Area Production in Supercritical, Transitional Mixing Layers
21 Low-Power, Zero-Vibration Sorption Coolers

BLANK PAGE

Characterization of Heat-Flux-Gauge Calibration System

Phenomena that affect measurements are being investigated in detail.

Dryden Flight Research Center, Edwards, California

A project is underway in the Flight Loads Laboratory (FLL) at Dryden Flight Research Center to reduce the uncertainties in heat-flux measurements. The impetus for this project is provided, in part, by the observation that uncertainties in heat-flux measurements are large — often 10 to 20 percent or more. Further impetus is provided by the fact that heat-flux calibration facilities being developed at the National Institute of Standards and Technology (NIST) operate at heat fluxes well below the levels which can be achieved during high-speed flight. Thus, a heat-flux-gauge user interested in such high fluxes has only two options: (1) take the gauge manufacturer's calibration on faith or (2) develop and understand his or her own calibration process.

The broad objectives of the project are:

- Characterize a radiant-heat-flux gauge-calibration system in the FLL (see Figure 1) in order to quantify and, if possible, reduce calibration uncertainty and
- Be able to demonstrate to customers that the FLL personnel understand the heat-flux-gauge calibrations that they perform.

The first phase of the project involves a thorough characterization of the calibration system, which uses an electrical resistance heated graphite plate as a heat source, in order to reach the first stated objective. Future phases of the project will involve development of methods for using gauges calibrated in this system in radiant-heating tests performed in the FLL and in flight.

The following is a partial list of technical challenges that must be met in the project:

- Determine the effects of erosion of graphite plates,
- Determine the effect of convection on the heat flux gauge, and
- Determine the effect, upon the distribution of absorbed heat flux, of the distance between a graphite plate and heat-flux gauge.

Thus far, an initial two-dimensional mathematical model of heat flux and temperature distribution has been developed for a vertical cross section of the graphite plate and heat flux gauge (see Figure 2). The rectangles in Figure 2 representing the graphite plate and heat flux gauge are in their proper relative positions and orientations but are not shown to scale. The results of initial experiments include heat fluxes within 10 percent of those predicted by the model. An initial graphite plate erosion model has predicted plate erosion within 5 percent of

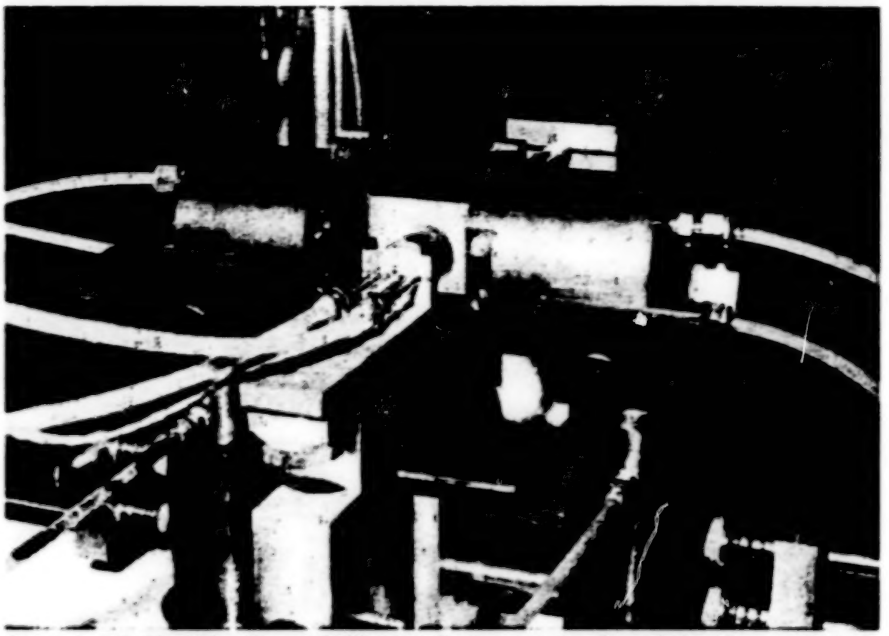

Figure 1. This Heat-Flux-Gauge Calibration System is to be characterized thoroughly, by a combination of experimental and theoretical means, as part of an effort to quantify and reduce calibration errors.

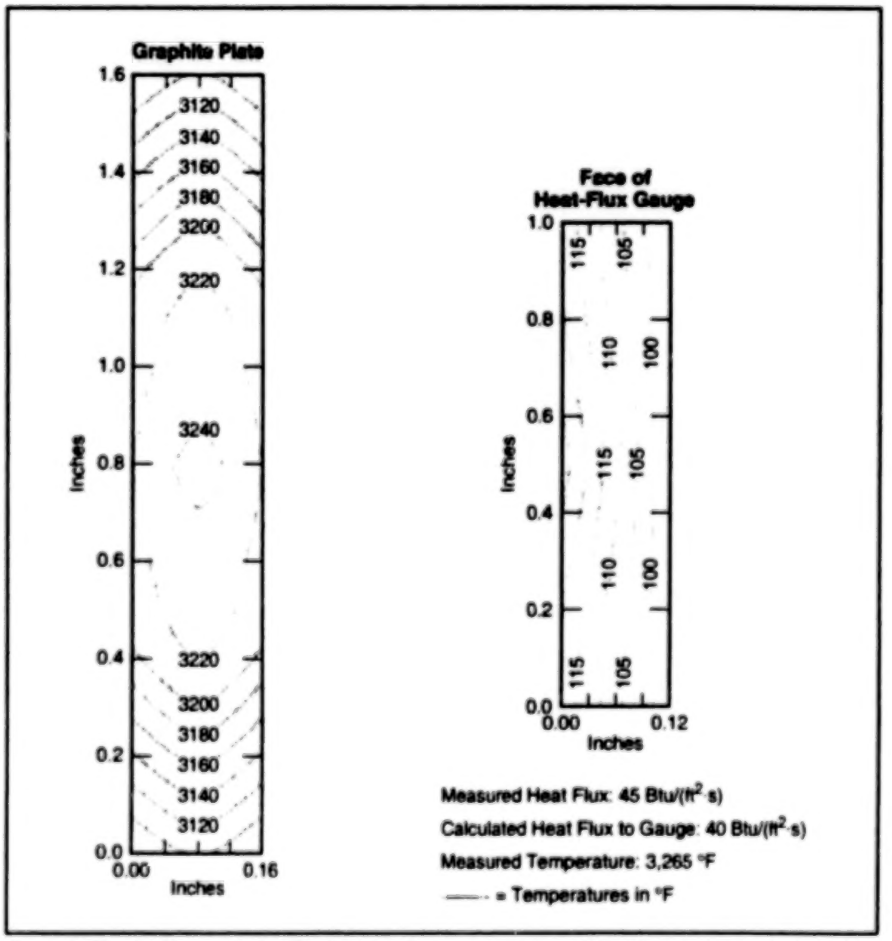

Figure 2. The Isotherms in the Rectangles that represent a graphite plate and a nearby heat-flux gauge were computed for a test case, by use of a two-dimensional mathematical model.

the measured values.

Planned future efforts include the following:

- Refinements of the two-dimensional model, including an improved erosion model and incorporating internal details of a circular foil heat flux gauge;
- Refinement of experiments to collect such additional detailed information as rates of flow and temperatures of gauge-cooling water and distributions of temperature in graphite plates;
- Expansion of the model to three dimensions; and
- Determination of experimental heat fluxes by use of alternative physical principles.

This work was done by Tom Horn of **Dryden Flight Research Center** *and Shanjuan Jiang and Vijay Dhir of the University of California. Further information is contained in a TSP [see page 1].*

DRC-98-77

Two-Fiber-Optic Method of Laser Doppler Velocimetry

Only one laser, instead of two, is needed.

John H. Glenn Research Center, Cleveland, Ohio

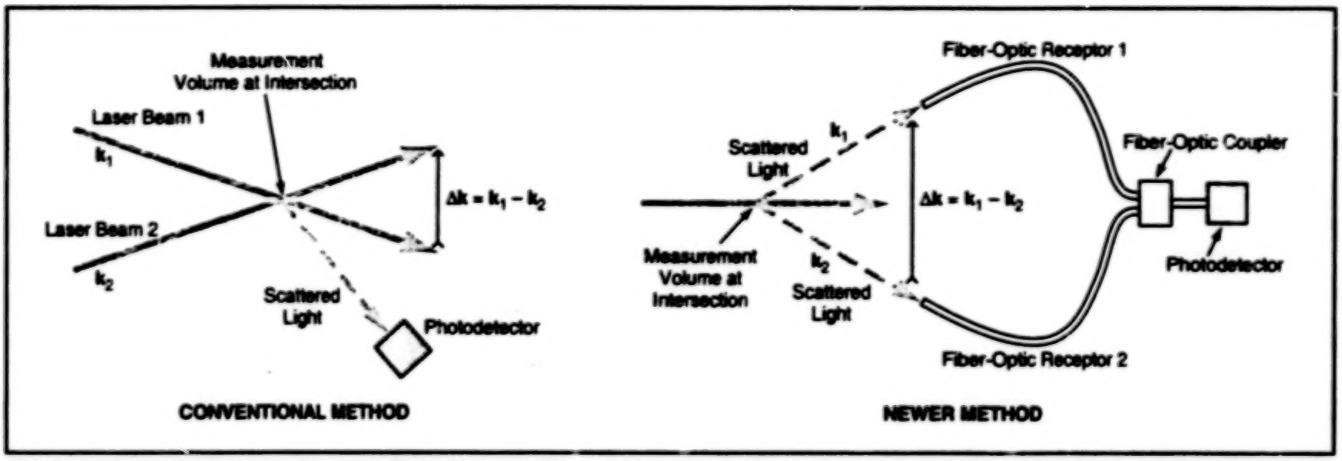

The Conventional Method and the Newer Method of LDV differ in, among other things, the manner of producing interference. In conventional LDV, the interference occurs between two laser beams in the small measurement volume. In the newer method, the interference takes place in the fiber-optic coupler and photodetector.

The figure depicts the basic optical layouts for (1) conventional laser Doppler velocimetry (LDV) and (2) a newer method of LDV based partly on the use of two optical fibers. Whereas conventional LDV involves the use of at least two lasers aimed in specified direction and detection of light scattered to one detector in almost any direction, the newer method involves only one laser and fiber-optic receptors that collected light scattered in two specified directions.

In conventional LDV, two coherent laser beams are made to intersect in a small measurement volume, where they interfere. As a seed particle entrained in a flow passes through the measurement volume, the laser light reflected by the particle is modulated at a frequency proportional to the spatial frequency of the interference fringes and the component of velocity perpendicular to the interference fringes. More specifically, the modulation frequency is given by $\Delta f = (1/2\pi)v \cdot \Delta k$, where v is the velocity and $\Delta k = k_1 - k_2$ is the difference between the wave vectors of the two laser beams. Because Δf is independent of the direction in which the light is scattered, a photodetector can be placed in any convenient position to receive the scattered light. The output of the photodetector is processed to extract Δf and thus the component of v in the $k_1 - k_2$ direction.

In the newer method, the measurement volume lies in a small region somewhere along a single illuminating laser beam, but in this case, the measurement volume lies at (and is defined by) the intersection of the laser beam and the lines of sight of two fiber-optic receptors. To obtain a high signal-to-noise ratio, these receptors are constructed in the form of polarization-preserving, single-mode optical fibers. Scattered light collected by these receptors is combined in a fiber-optic coupler and delivered to a photodetector, where interference between the beams scattered in the two directions gives rise to a Doppler beat frequency. This beat frequency is given by the same equation as that for the modulation frequency in conventional LDV, except that in this case, $\Delta k = k_1 - k_2$ is the difference between the wave vectors (at the laser wavelength) defined by the lines of sight from the measurement volume to the input ends of the two fiber-optic receptors. In this case, Δf is independent of the direction of the laser beam; hence, it is possible to illuminate the measurement volume from any convenient direction. The beat frequency can be measured by use of a standard LDV signal processor, a commercial digital photon correlator, or a fast digital correlator.

Unlike in conventional LDV, it is not necessary to add more lasers operating at different wavelengths and aimed in different directions in order to be able to measure additional velocity components. Instead, it suffices to add pairs of fiber-optic receptors aimed to define the corresponding orthogonal wave-vector differences, plus the signal-processing equipment needed to extract the beat-frequency outputs of the additional receptors.

This work was done by Penger Tong, Bruce J. Ackerson, and Walter I. Goldburg of Oklahoma State University for **Glenn Research Center.**

Inquiries concerning rights for the commercial use of this invention should be addressed to NASA Glenn Research Center, Commercial Technology Office, Attn: Steve Fedor, Mail Stop 4–8, 21000 Brookpark Road, Cleveland, Ohio 44135. Refer to LEW-17136.

Software for Electromagnetic Detection of Buried Explosives

Data from a variety of sensors on different survey grids can be used.

NASA's Jet Propulsion Laboratory, Pasadena, California

U-HUNTER (also called "UXO-HUNTER") is a computer program that affords knowledge-based real-time sensor-fusion and display capabilities for detecting buried objects and materials of interest. U-HUNTER is intended especially for inferring the presence of buried unexploded ordnance and explosive waste from the readings of magnetic and electromagnetic sensors like those commonly used in geophysical surveys. U-HUNTER is also potentially adaptable to such other uses as detection of mines, medical imaging and diagnosis, detecting and monitoring buried pipes and cables, environmental monitoring, and geological surveys.

U-HUNTER can utilize data in a wide variety of formats. At present, it can accept and process the data from such sensors as magnetometers, synthetic-aperture radar systems, and time-domain pulsed eddy-current sensors. U-HUNTER has the potential for reducing (in comparison with prior sensor-data-analysis software) the rate of errors in the detection of anomalies (that is, unexploded ordnance or other phenomena of interest). U-HUNTER also has the potential for enabling better characterization and classification of detected anomalies. Envisioned applications of U-HUNTER include not only analysis of fresh data from continuing surveys but also re-evaluation of historical survey data to increase the level of certainty of detection of unexploded ordnance at sites where such surveys have already been performed. Fusion of multiple-sensor and/or multiple-survey data from the same site is also envisioned.

U-HUNTER contains unique subsystems that perform different functions, as follows:

- A data-enhancement subsystem preprocesses input data to condition them for analysis. One of the most powerful features of U-HUNTER is a fully integrated programming interface within the data-enhancement subsystem. This interface makes it possible to develop custom algorithms to preprocess and display the data to be fed as input to the analysis-engine subsystem mentioned below. U-HUNTER is flexible enough to allow the import of any image or raw matrix data for analysis. This capability alone has proven to be most impressive in enabling users familiar with data from sensors of one type (e.g., magnetometers) to apply the analytical capabilities of U-HUNTER to data from sensors of another type (e.g., synthetic-aperture radar).
- An analysis-engine subsystem includes a version of ARTMAP, which is part of a previously developed neural-network software system. The analysis-engine subsystem is also expected to include ANFIS — a yet-to-be-developed program for implementing an adaptive neuro-fuzzy information software system for a secondary method of classification of anomalies.
- A subsystem called "3DKB" is dedicated to facilitation of the assimilation of the items of a three-dimensional knowledge base. The 3DKB items comprise the knowledge built up by a user from ground-truth data for the purposes of training neural and neuro-fuzzy software components within U-HUNTER. Dialog-type displays enable users to load 3DKB items for training of the ARTMAP-type neural networks for classification of anomalies.
- A visualization subsystem generates displays of geophysical data on three-dimensional-appearing surface models and two-dimensional color maps. The maps provide a capability for rapid visual inspection of a surveyed area. Deep-blue dots are placed at locations of local maxima of and magenta dots are placed at locations of local minima of quantities of interest. The user can customize maximum- and minimum-finding algorithms to obtain desired levels of discrimination. A subprogram called "3D Anomaly Viewer" enables users to see the shapes of found anomalies.

U-HUNTER has been found to perform robustly, both (1) when applied in real time at the survey-grid-interval level (<100 m by <100 m) and (2) when applied at the entire-site level after completion of surveys of sites ranging in size from 500 to 25,000 acres (2 to 100 km^2). U-HUNTER enables detection of anomalies at the 100-percent level, while keeping the incidence of false alarms down to the 2-percent level. It also provides for robust generalization to new sites without additional training or setup, and it minimizes the effect of reacquisition of data on post-processing. It can perform robustly despite poor ground control; that is, it can tolerate errors of the order of grid intervals. Furthermore, U-HUNTER enables rapid synthetic resampling and interpolation of data to a spatial resolution relevant to the spatial distribution of unexploded ordnance, and enables resampling of data from multiple sensors to a common spatial scale.

Planned future development of U-HUNTER includes an extension of data-display capabilities to provide for overlays of planimetric data, aerial photography, and geophysical data. Other planned enhancements include extension of analysis subsystems to accommodate additional alterative classification methods and development of an improved user interface to make the U-HUNTER more accessible to the general geophysical community.

This work was done by Sandeep Gulati and Vijay Deggumati of Caltech for ***NASA's Jet Propulsion Laboratory****. Further information is contained in a TSP [see page 1].*

This software is available for commercial licensing. Please contact Don Hart of the California Institute of Technology at (818) 393-3425. Refer to NPO-20808.

Aircraft Anti-Icing Systems Utilizing Induced Hydrophobicity

It should be possible to build lightweight, low-power, low-profile anti-icing systems based on this concept.

John H. Glenn Research Center, Cleveland, Ohio

Aircraft anti-icing systems of a proposed type would utilize static electric fields to reduce or eliminate the electrostatic forces that bond ice and water to metal surfaces. These would be lightweight, low-power-consumption, inexpensive systems that would be installed on the surfaces of wings and other critical airfoils. These systems would not intrude significantly into

the interiors of airfoils; they would also not protrude from airfoil surfaces and thus would not disturb aerodynamics.

Many anti-icing systems now in common use are of the "weeping-wing" type: they mete out deicing fluids over airfoils. The reservoirs needed to store deicing fluids, the plumbing needed to distribute the fluids over the airfoil surfaces, and the fluids themselves impose severe interior-space and weight penalties on aircraft design and operation, and the fluids can exert adverse effects on the environments into which they are released. Some other anti-icing systems now in use are of the electrothermal type; the disadvantage of these systems is that they consume significant amounts of aircraft power. Yet another anti-icing concept that has been tried previously involves the use of such ice-phobic materials as polytetrafluoroethylene; this concept has met only limited success, and performance can be degraded through erosion of ice-phobic materials.

Three phenomena that contribute to the adhesion of ice are electrostatic attraction, covalent bonding, and the Van der Waals force. The electrostatic force is possibly the most significant. Because water and ice are polar materials, the alignment of their molecules is influenced by an electric field. Water adheres to a metallic surface because the molecular orientation is such that a positive charge exists on the water surface facing the metal and is attracted to a negative charge on the metal surface. On freezing, water molecules reorganize from a liquid to a crystalline structure that remains polar. Thus, ice adheres to the metal surface for the same reason that water does. In principle, the electrostatic part of the bonding force could be eliminated by applying an opposing dc electric field across the interface between the metal surface and the ice. In the proposed systems, the necessary electric fields would be generated by use of electrodes patterned on the airfoil surfaces to be protected. The fundamental research on the reduction of ice adhesion strength using an applied dc electric charge was conducted by Professor Victor Petrenko of Dartmouth's Thayer School of Engineering. Dartmouth College has patented the technology (U.S. Patent No. 6,027,075).

Systems of the proposed type would be attractive for use on general aviation and commuter aircraft. These systems could provide safety margins for aircraft that inadvertently encounter icing conditions. An electrostatic anti-icing system could be activated prior to entering actual or potential icing conditions, without power or performance penalty. An electrostatic anti-icing system could also enhance the performance of an electro-expulsive or pneumatic-boot deicer by reducing or eliminating residual ice after each activation of the deicer.

This work was done by Jack Edmonds and Richard B. Ingram of Innovative Dynamics, Inc., for **Glenn Research Center**.

Inquiries concerning rights for the commercial use of this invention should be addressed to NASA Glenn Research Center, Commercial Technology Office, Attn: Steve Fedor, Mail Stop 4–8, 21000 Brookpark Road, Cleveland, Ohio 44135. Refer to LEW-16939.

Books and Reports

Paraffin-Actuated Heat Switch for Mars Surface Applications

Missions to the surface of Mars pose unique thermal-control challenges to rover and lander systems. With diurnal temperature changes greater than 100 °C, the presence of a Mars atmosphere, and limited power for night-time heating, the thermal-control engineer is faced with a fundamental problem: how to successfully keep components above their survival or operating temperatures at night while managing higher environmental temperatures and dissipation rates during the day. Payload and avionics elements, among others, must be well insulated to survive night conditions at the risk of overheating during the day. This problem will be magnified in future missions as higher demand on electrical components will result in increased dissipations. One solution is a heat switch that changes thermal conductance to reject excess heat during the day and conserve heat during the night. A report describes such a paraffin-actuated heat switch as part of the thermal-control system for a robotic exploratory vehicle on Mars. Over a predetermined temperature range, the switch heat conductance varies by nearly two orders of magnitude to regulate temperatures. The actuation of the heat switch is entirely mechanical and autonomous, relying on the temperature based expansion and contraction of paraffin contained in a seal boot.

This work was done by Keith S. Novak, Gajanana Birur, Eric Sunada, Michael Pauken, Charles Phillips, and Donald Sevilla of Caltech and Kurt Lankford of Starsys Research Corporation for **NASA's Jet Propulsion Laboratory**. *To obtain a copy of the report, "Paraffin Actuated Heat Switch for Mars Surface Applications," see TSP's [page 1].*
NPO-30351

Inhibited Carrier Transfer in Ensembles of Quantum Dots

A report presents an experimental study of time-resolved, temperature-dependent photoluminescence in $In_xGa_{1-x}As/GaAs$ specimens containing $In_{0.6}Ga_{0.4}As$ quantum dots (QDs) distributed at several different areal densities on a GaAs surface and capped with GaAs. The specimens were fabricated by metal-organic vapor deposition of $In_xGa_{1-x}As$ on slightly misoriented, semi-insulating GaAs(100) substrates. At high areal densities, the intensities of photoluminescence from the QDs were found to exhibit Arrhenius temperature dependence, attributed to thermal emission of charge carriers and recapture of the charge carriers into neighboring QDs. At low densities, it was found that the temperature dependence is more complex, the thermal transfer of charge carriers between neighboring QDs plays no significant role in the temperature dependence, and the efficiency of transfer of charge carriers into isolated QDs is limited by the rate of carrier transport in $In_xGa_{1-x}As$ wetting layers. The results of time-resolved measurements of photoluminescence — in particular, the temperature and excitation-power dependences of the rise time of the photoluminescence from isolated QDs — were found to be consistent with the interpretation of the temperature dependence of intensity upon charge-carrier-transfer mechanisms in the wetting layers. Differences in carrier transport between high- and low-surface-density QD samples were explained by strain induced potential barriers surrounding the QDs. These potential barriers inhibit carrier capture at low temperature in low-density QD samples.

This work was done by Rosa Leon and Charlene Lobo of Caltech for **NASA's Jet Propulsion Laboratory**. *To obtain a copy of the report, "Inhibited carrier transfer in ensembles of isolated quantum dots," see TSP's [page 1].*
NPO-21029

Area Production in Supercritical, Transitional Mixing Layers

This paper presents a study of area production in mixing layers undergoing transition to turbulence. These layers evolve from the mixing of two initially segregated counterflowing streams under supercritical conditions. The study may contribute to development of means to control area production in order to increase disintegration of fluids and enhance combustion in diesel, gas turbine, and liquid rocket engines. As used here, "area production" signifies the fractional rate of change of surface area oriented perpendicular to the mass-fraction gradient in a mixing layer. In the study, a database of transitional states obtained from direct numerical simulations of temporal three-dimensional supercritical mixing layers for heptane/nitrogen and oxygen/hydrogen systems was analyzed. A few of the many conclusions drawn from the analysis are that area production is determined more by strain than by compressibility; area is produced by strain and convective effects; area is destroyed by species mass flux, rotational effects, and pressure gradients; area can be either produced or destroyed by pressure gradients; and effects of viscosity on area production are negligible. Effects of departure from perfect-gas and ideal-mixture behavior were found to be important. Smaller-wavelength initial perturbations were found to lead to greater area production: this observation could be a guide to initial development of control of area production.

This work was done by Josette Bellan and Nora Okong'o of Caltech for **NASA's Jet Propulsion Laboratory**. *To obtain a copy of the paper, "Area Production in Supercritical, Transitional Mixing Layers for Reactive Flow Applications," see TSP's [page 1].*

NPO-30425

Low-Power, Zero-Vibration Sorption Coolers

A report discusses three designs of proposed low-power, zero-vibration coolers for infrared instruments planned to be flown aboard spacecraft to perform astrophysical observations far from Earth. The designs take advantage of the radiative precooling available in the projected deep-space operational environments: such precooling makes it possible to reach radiator temperatures as low as tens of kelvins. The working fluids would be helium and hydrogen, and vibration would be eliminated by the choice of thermally cycled gas-sorption (hydrogen/metal hydride and helium/charcoal) units instead of mechanical compressors. The first design calls for a helium/charcoal lower-temperature stage and an $H_2/La_{4.78}Sn_{0.22}$ higher-temperature stage, which would dump heat to a radiator at 260 K. The second design combines a helium/charcoal stage with a hydrogen/charcoal stage. It takes significant advantage of the environment through radiant cooling of the hotter stage at 50 K. The third design utilizes three charcoal cooling stages. Helium, hydrogen, and neon are used as refrigerants in these stages. This system also relies on radiant cooling of the hottest stage at 60 K. Each cooler would be sized to provide 2 mW of net refrigeration power at a temperature of 5 K and 10 mW at 16.5 K. Each cooler would have a mass <10 kg and input power demand between 2 and 25 W.

This work was done by Lawrence Wade and Christian Lindensmith of Caltech for **NASA's Jet Propulsion Laboratory**. *To obtain a copy of the report, "Low-Power, Zero-Vibration 5K Sorption Coolers for Astrophysics Instruments," see TSP's [page 1].*

NPO-30369

BLANK PAGE

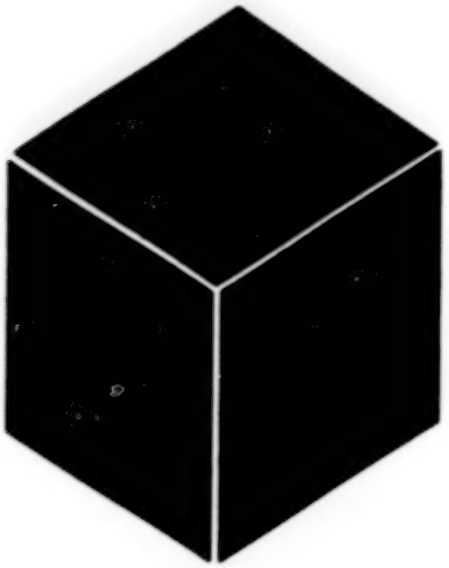

Materials

Hardware, Techniques, and Processes

25 Chevrel Phases as Potential Thermoelectric Materials
25 Composite-Material Structures for Absorbing Crash Energy
26 Alkyl Pyrocarbonate Electrolyte Additives for Li-Ion Cells
27 Fluorinated Alkyl Carbonates as Cosolvents in Li-Ion Cells
28 Diaminobenzoquinones as Corrosion-Inhibiting Additives
29 Improved Conversion Coating for Protection of Metals

Books and Reports

29 Nanolaminate Mirrors With Integral Figure-Control Actuators

BLANK PAGE

Chevrel Phases as Potential Thermoelectric Materials

Scattering of phonons by loosely bound atoms reduces thermal conductivity.

NASA's Jet Propulsion Laboratory, Pasadena, California

Crystalline phases of compounds of general composition (Cu_w, Cu_xFe_y, or $Ti_zMo_6Se_8$ [where $w<4$, $x<2$, $y<1$, and $z<1$] have been investigated for potential utility as thermoelectric materials for generation of electric power from waste-heat and other thermal sources. These phases are a subset of a set of ternary chalcogenide compounds named Chevrel compounds or phases after one of the researchers who first synthesized them in 1971. As explained below, relatively low thermal conductivity is an outstanding aspect of these compounds that makes them potentially attractive for thermoelectric applications.

The figure of thermoelectric merit of a given material at a given temperature T is commonly denoted as ZT and is given by the equation $ZT = \alpha^2 T/\rho\lambda$, where α is the Seebeck coefficient, ρ is the electrical resistivity, and λ is the thermal conductivity of the material at that temperature. Hence, as part of an effort to develop a material of large ZT, one should seek to minimize λ.

The present investigation is an extension of recent research on other thermoelectric materials that belong to a class of compounds called "rattling" semiconductors. The crystalline lattices of these materials contain cavities large enough to accommodate a variety of additional atoms, which are bound relatively loosely and are thus somewhat free to move around ("rattle"). It had been suggested that in such compounds, the rattling of the additional atoms would contribute more to scattering of phonons than to scattering of electrons and holes. Consequently, the rattling could be expected to contribute more to thermal than to electrical resistivity — an effect that would be favorable for obtaining a large value of ZT.

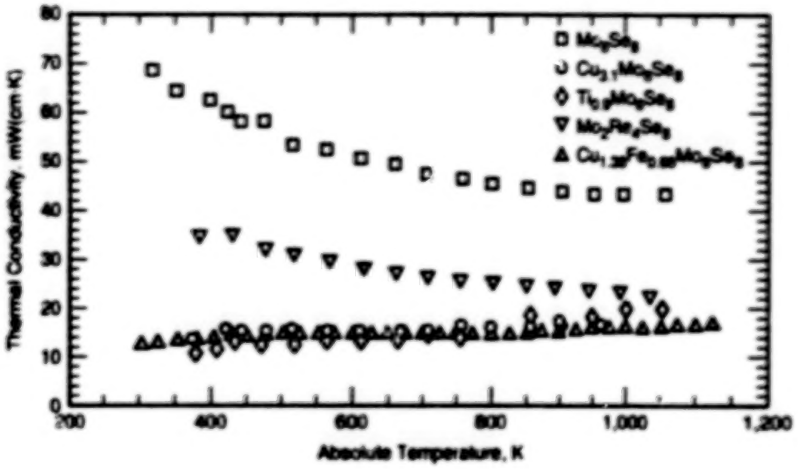

Thermal Conductivities (as functions of temperature) of several candidate Chevrel phases were measured. Also shown for comparison are the corresponding quantities for Mo_6Se_8 and $Mo_2Re_4Se_8$.

The Cu_w, Cu_xFe_y, or $Ti_zMo_6Se_8$ Chevrel phases belong to the class of rattling materials. The electronic and thermal properties of these compounds could, potentially, be tailored through careful selection of the amounts and the manner of incorporation of the filling elements (Cu, Cu with Fe, or Ti). The compounds investigated thus far are $Cu_{3.1}Mo_6Se_8$, $Cu_{1.35}Fe_{0.65}Mo_6Se_8$, and $Ti_{0.9}Mo_6Se_8$, which exhibit p-type electrical conductivity and relatively low values of thermal conductivity (see figure). Of these compounds, the best was found to be $Cu_{1.35}Fe_{0.65}Mo_6Se_8$, for which $ZT = 0.6$ at a temperature of 1,150 K. This value of ZT is comparable to the ZT values of Si-Ge alloys in the same temperature range. One drawback of these three compounds has been low charge-carrier mobility. It will be necessary to increase charge-carrier mobilities in order to obtain ZT values greater than those of state-of-the-art thermoelectric materials. Research toward that end was underway at the time of reporting the information for this article.

This work was done by Thierry Caillat, Jean-Pierre Fleurial, G. Jeffrey Snyder, and Alexander Borshchevsky of Caltech for **NASA's Jet Propulsion Laboratory**. *Further information is contained in a TSP [see page 1].*

In accordance with Public Law 96-517, the contractor has elected to retain title to this invention. Inquiries concerning rights for its commercial use should be addressed to

Technology Reporting Office
JPL
Mail Stop 249-103
4800 Oak Grove Drive
Pasadena, CA 91109
(818) 354-2240

Refer to NPO-21012, volume and number of this NASA Tech Briefs *issue, and the page number.*

Composite-Material Structures for Absorbing Crash Energy

These structures can be fabricated relatively easily and inexpensively.

Langley Research Center, Hampton, Virginia

Improved lightweight composite-material structures have been invented to protect persons and equipment during aircraft and ground-vehicle crashes. These structures are designed to hold their initial shapes and sustain rated loads under normal operating conditions and, during crashes, to undergo sustained deformation with high stroke efficiency at tailored crush loads to absorb kinetic energy. The advantages offered by these structures over prior crash-energy-absorbing structures, including composite-material ones, are that these structures can be fabricated by use of relatively simple, cost-effective techniques and the designs of the structures can readily be adapted to a variety of applications.

One example of design and fabrication of a structure of this type is that of a simple rectangular parallelepiped beam comprising a stack of cells (see figure). The cell cores are designed to be crushed along their longest axes. First, the cells are fabricated, starting from blocklike cores, which

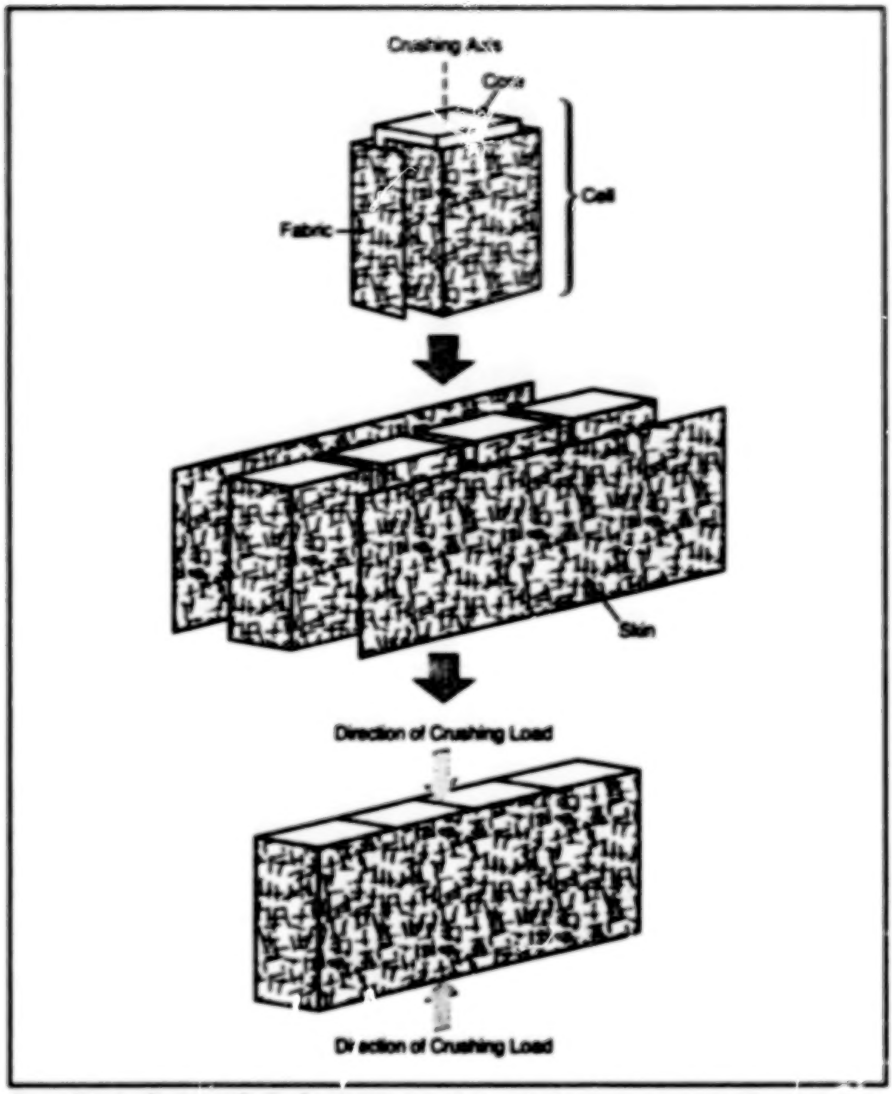

Foam Blocks Designed To Be Crushable along their vertical axes are wrapped with resin-impregnated fabric, then stacked horizontally. The stack is overwrapped with another resin-impregnated fabric, and the resins are cured to form a unitary beam.

could be hollow and/or made from a closed-cell, low-density, rigid polymeric structural foam. Each core is wrapped with a woven fabric or other continuous fiber reinforcement. The wrap is impregnated with a suitable matrix resin by use of any of a number of established techniques.

The cells are stacked in the desired orientation along the intended longitudinal axis of the beam. In a typical application, the beam might be intended to serve as a subfloor structure in an aircraft, where it could protect occupants against excessive vertical crash loads by yielding vertically; in this case, the preferred orientation of the long axis of each cell in the stack is vertical. Skins of resin-impregnated continuous fiber reinforcement, possibly similar to those of the individual cells, are wrapped around the stack, holding the cells together firmly. Then the resins are cured, yielding a unitary, rigid structure, wherein the bonded skins at the interfaces of adjoining cells constitute additional transverse reinforcements. If there is a requirement that the beam retain its post-crash integrity, then the skin should be composed of tough fibers (e.g., an aromatic polyamide or polyethylene fabric).

Structures of this type are not limited to a simple beam design and fabrication sequence like those described above. Structures can have more complex regular or irregular shapes, can be fabricated in different sequences, and can be made from different foams, fibers, and resins. The materials, dimensions, fiber orientations, and other design parameters can be selected to obtain specified direction-dependent crushing characteristics while satisfying shape and load-bearing structural requirements during normal operation.

This work was done by Sotiris Kellas for and Huey Carden of **Langley Research Center**. *Further information is contained in a TSP [see page 1].*

This invention has been patented by NASA (U.S. Patent No. 5,746,537). Inquiries concerning nonexclusive or exclusive license for its commercial development should be addressed to Rheal Turcotte, Technology Commercialization Program Office, NASA Langley Research Center at (757) 864-8881 or e-mail at r.p.turcotte@larc.nasa.gov. Refer to LAR-15397.

Alkyl Pyrocarbonate Electrolyte Additives for Li-Ion Cells

Beneficial properties of films that form on carbon anodes are enhanced.

NASA's Jet Propulsion Laboratory, Pasadena, California

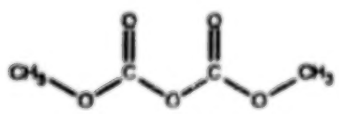

Dimethyl Pyrocarbonate

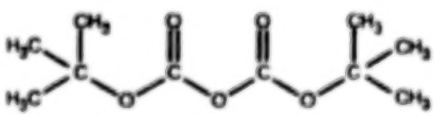

Di-(*t*-Butyl) Pyrocarbonate

These Alkyl Pyrocarbonates, when used as additives to an optimized electrolyte formulation, have been found to improve the low-temperature performances of rechargeable lithium-ion cells by contributing to the formation of protective SEIs with increased ionic conductivities.

Alkyl pyrocarbonates have been found to be useful as electrolyte additives for improving the low-temperature performances of rechargeable lithium-ion electrochemical cells. The beneficial effects of these and other additives have been investigated, along with various electrolyte formulations, in continuing research directed toward extending the range of practical operating temperatures from the present lower limit of –20 °C down to –40 °C, and even lower if possible. This research at earlier stages was reported

in a number in *NASA Tech Briefs* articles; namely, "Update on Electrolytes for Low-Temperature Lithium Cells," (NPO-20407), January 2000; "Lithium Alkoxide Electrolyte Additives for Lithium-Ion Cells" (NPO-20607), June 2001; "Aliphatic Ester Electrolyte Additives for Lithium-Ion Cells" (NPO-20601), June 2001; and "Ethyl Methyl Carbonate as a Cosolvent for Lithium-Ion Cells" (NPO-20605), June 2001.

To recapitulate from the cited prior articles: the loss of performance with decreasing temperature is attributable largely to a decrease of ionic conductivity and the increase in viscosity of the electrolyte. What is needed to extend the minimum operating temperature from –20 °C down to –40 °C is a stable electrolyte solution with relatively small low-temperature viscosity, a large electric permittivity, adequate coordination behavior, and appropriate ranges of solubilities of liquid and salt constituents. Whether the anode is made of graphitic or non-graphitic carbon, the surface film acts as a solid/electrolyte interface (SEI), the nature of which is critical to low-temperature performance. Desirably, the surface film should exert a chemically protective effect on both the anode and the electrolyte, yet should remain conductive to lithium ions to facilitate intercalation and deintercalation of the ions into and out of the carbon during discharging and charging, respectively.

One previously reported optimized electrolyte formulation is a 1.0 M solution of $LiPF_6$ in a ternary solvent that consists of equal volume parts of ethylene carbonate (EC), dimethyl carbonate (DMC), and diethyl carbonate (DEC). Also previously reported is the use of customary additives to this baseline optimized formulation to enhance low-temperature performance.

The present alkyl pyrocarbonate additives (see figure) to the baseline optimized electrolyte formulation promote the formation of protective and conductive SEIs on carbon anodes. The formation of such SEIs is believed to be facilitated by products (e.g., CO_2) of the decomposition of these additives. These decomposition products are believed to react to form Li_2CO_3-based films on the carbon electrodes. The improvement (relative to the baseline formulation) in interfacial properties resulting from the use of these additives is more evident at low temperature, where enhanced kinetics of intercalation and deintercalation of Li, higher ionic transport across SEIs, and increased discharge capacities with low overpotentials are observed. Also, the SEIs that form in the presence of these additives are more stable toward any further reduction of the electrolyte and thus more stable against growth to greater thicknesses; hence, they contribute to the cycle lives of the anodes.

This work was done by Marshall Smart, Ratnakumar Bugga, and Subbarao Surampudi of Caltech for **NASA's Jet Propulsion Laboratory**. *Further information is contained in a TSP (see page 1).*

In accordance with Public Law 96-517, the contractor has elected to retain title to this invention. Inquiries concerning rights for its commercial use should be addressed to

Intellectual Property group
JPL
Mail Stop 202-233
4800 Oak Grove Drive
Pasadena, CA 91109
(818) 354-2240

Refer to NPO-20775, volume and number of this NASA Tech Briefs issue, and the page number.

Fluorinated Alkyl Carbonates as Cosolvents in Li-Ion Cells

These solvents offer advantages with respect to performance and safety.

NASA's Jet Propulsion Laboratory, Pasadena, California

Partially fluorinated alkyl carbonate liquid compounds have been found to be excellent electrolyte cosolvents for rechargeable lithium-ion electrochemical cells. The benefits afforded by these and other ingredients of electrolyte solutions in rechargeable Li-ion cells have been investigated in continuing research directed toward extending the range of practical operating temperatures of the cells (from +40 °C down to –40 °C, and possibly even as low as –60 °C). Fluorinated solvents were perceived to be especially attractive in that they will result in inherently safer cells, due to their low flammability. This research at earlier stages was reported in a number of *NASA Tech Briefs* articles; namely, "Update on Electrolytes for Low-Temperature Lithium Cells" (NPO-20407), January 2000; "Lithium Alkoxide Electrolyte Additives for Lithium-Ion Cells" (NPO-20607), June 2001; "Aliphatic Ester Electrolyte Additives for Lithium-Ion Cells" (NPO-20601), June 2001; "Ethyl Methyl Carbonate as a Cosolvent for Lithium-Ion Cells" (NPO-20605), June 2001; and "Alkyl Pyrocarbonate Electrolyte Additives for Li-Ion Cells" (NPO-20775), this issue, preceding article.

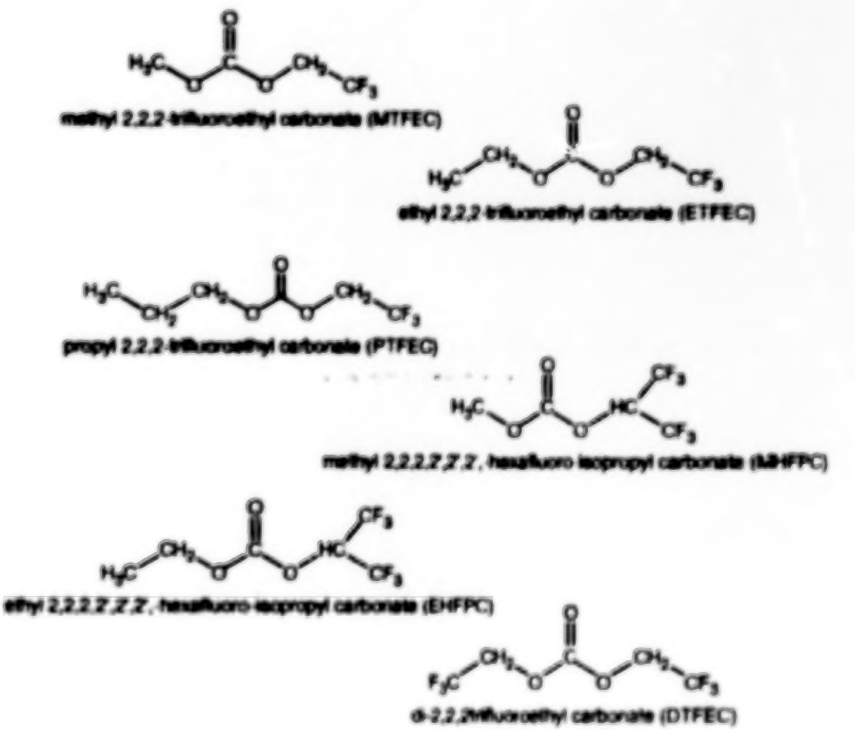
methyl 2,2,2-trifluoroethyl carbonate (MTFEC)
ethyl 2,2,2-trifluoroethyl carbonate (ETFEC)
propyl 2,2,2-trifluoroethyl carbonate (PTFEC)
methyl 2,2,2,2',2',2'-, hexafluoro isopropyl carbonate (MHFPC)
ethyl 2,2,2,2',2',2'-, hexafluoro-isopropyl carbonate (EHFPC)
di-2,2,2-trifluoroethyl carbonate (DTFEC)

These Partially Fluorinated Alkyl Carbonates were tested as electrolyte cosolvents for rechargeable Li-ion cells.

The partially fluorinated carbonate cosolvents and the electrolytes formulated by use of these solvents were evaluated in comparison with baseline (nonfluorinated) alkyl carbonate cosolvents and the corresponding baseline electrolyte formulation. The baseline mixture of cosolvents consists of equal volume parts of ethylene carbonate (EC), dimethyl carbonate (DMC), and diethyl carbonate (DEC). The baseline electrolyte formulation is a 1.0 molar solution of lithium hexafluorophosphate ($LiPF_6$) in the baseline mixture of cosolvents.

The partially fluorinated carbonate solvents studied (see figure) include:

- methyl 2,2,2-trifluoroethyl carbonate (MTFEC),
- ethyl 2,2,2-trifluoroethyl carbonate (ETFEC),
- propyl 2,2,2-trifluoroethyl carbonate (PTFEC),
- methyl 2,2,2,2′,2′,2′-hexafluoro-isopropyl carbonate (MHFPC),
- ethyl 2,2,2,2′,2′,2′-hexafluoro-isopropyl carbonate (EHFPC), and
- di-2,2,2-trifluoroethyl carbonate (DTFEC).

Ternary and quaternary mixtures containing various combinations of these cosolvents were used to formulate electrolytes containing $LiPF_6$ at concentrations of 0.5, 0.75, and 1.0 molar.

The fluorinated carbonate cosolvents exhibit the requisite chemical stability of the baseline cosolvents while offering more desirable physical properties imparted by the presence of the fluorine substituents. These more desirable properties include: (1) lower melting temperatures; (2) greater chemical and electrochemical stability; (3) lower intermolecular forces and lower polarizability, which result in lower surface energies; and (4) lower flammability and thus greater safety.

Laboratory test cells constructed with these electrolytes exhibited high capacities at temperatures from −20 °C to −40 °C, capability for high rates of charge and discharge at low temperatures, and low electrode polarization. Hence, these electrolytes appear to be useful for constructing rechargeable lithium-ion cells with high specific energies, long lifetimes, and ability to function well at low temperatures.

This work was done by Marshall Smart, Ratnakumar Bugga, Subbarao Surampudi, Surya Prakash, and Jinbo Hu of Caltech for **NASA's Jet Propulsion Laboratory**. *Further information is contained in a TSP [see page 1].*
NPO-21076

Diaminobenzoquinones as Corrosion-Inhibiting Additives

Protection can extend beyond edges of paints to adjacent unpainted areas.

John F. Kennedy Space Center, Florida

Non-polymeric N,N′-di-N-hydrocarbyl-2,5-diamino-1,4-benzoquinones (where the hydrocarbyl substituents are alkyl or aryl) have been found to be useful as corrosion-inhibiting additives for paints and other conventional coating materials that are applied to steel and other metals. Prior coating additives made from reactions of benzoquinones with diamines are polymeric. Such polymers are expensive and difficult to make. Moreover, being polymers, they cannot diffuse much and hence are believed not to protect uncoated areas of metal against corrosion. In contrast, when used in proper concentrations, the present non-polymeric diaminobenzoquinones provide enhanced protection that extends somewhat from the edges of coats into uncoated areas — an important advantage in situations in which there are imperfections (e.g., gaps, scratches, and blisters) in coats of paint.

The figure depicts the generic molecular structure and lists examples of the present corrosion-inhibiting compounds. Each of these compounds is synthesized from 1,4-benzoquinone and the corresponding amine. In those listed compounds that contain NH groups, the reactivity of the NH groups is attenuated by the attached electron-poor quinone structures; consequently, those compounds are practically unreactive under normal conditions for curing coating materials, so that the compounds behave as additives, not reactives.

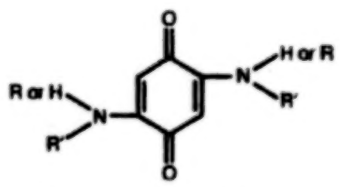

EXAMPLES OF COMPOUNDS
2,5-di(methylamino)-1,4-benzoquinone
2,5-di(butylamino)-1,4-benzoquinone
2,5-di(dodecylamino)-1,4-benzoquinone
2,5-di(allylamino)-1,4-benzoquinone
2,5-di(cyclohexylamino)-1,4-benzoquinone
2,5-di(methoxyethylamino)-1,4-benzoquinone
2,5-diphenylamino-1,4-benzoquinone
2,5-di-*p*-tolylamino-1,4-benzoquinone
2,5-di(4-dodecylphenylamino)-1,4-benzoquinone
2,5-di(methoxyphenylamino)-1,4-benzoquinone
2,5-di(dodecylamino)-1,4-benzoquinone
2,5-di(dimethylamino)-1,4-benzoquinone
2,5-di(N-methyl-N-cocoamino)-1,4-benzoquinone
2,5-dimorpholinyl-1,4-benzoquinone

In a Generic Corrosion-Inhibiting Compound of the present type, each of R and R′ is an alkyl, cycloalkyl, alkenyl, cycloalkenyl, or aryl group that is either unsubstituted or substituted with alkoxy or other non-polymer-reactive groups.

Unlike prior functionally substituted or polymeric diaminobenzoquinones, the present corrosion inhibitors are not limited to use in coating materials based on a particular family of polymers. Examples of types of coating materials to which the present compounds can be added for effective protection against corrosion include acrylics, polyesters, alkyds, polyamides, epoxies, phenolics, aminoplastics, polyimides, urethanes, silicones, and coating materials based on unsaturated drying oils.

The preferred amounts of these compounds lie in the range from 2 to 15 weight percent of coating solids. In each case, the chosen additive of this type is dissolved in the coating material (insofar as it is soluble) before the coating material is applied to steel. Alternatively or in addition, insofar as the additive is insoluble, it is dispersed into the coating material in finely powdered form. The standard paint-making techniques and materials can all be used in conjunction with the present corrosion-inhibiting compounds. In addition, the present corrosion-inhibiting compounds can be included in paints and other coating materials together with other corrosion-inhibiting compounds, such as chromates, molybdates, borates, and carbonates.

This work was done by Edward D. Weil of Polytechnic University for **Kennedy Space Center**. *Further information is contained in a TSP [see page 1].*

This invention is owned by NASA, and a patent application has been filed. Inquiries concerning nonexclusive or exclusive license for its commercial development should be addressed to the Technology Programs and Commercialization Office, Kennedy Space Center, (321) 867-6373. Refer to KSC-11979.

Improved Conversion Coating for Protection of Metals

This method is an environmentally friendly alternative to older processes.

John H. Glenn Research Center, Cleveland, Ohio

A simple, cost effective, environmentally friendly conversion-coating process has been developed for protecting a variety of metals against wear and corrosion and to increase adhesion of paints. This process results in the deposition of a thin, adherent coats of iron phosphate on treated metal substrates. This process is expected to supplant the environmentally hazardous chromate-based conversion-coating process heretofore used in the automotive and aerospace industries. It is also expected to supplant a process in which bearing races made of 440C stainless steel are pretreated with tricresyl phosphate.

In the improved process, a predeaned metal substrate of 440C stainless steel or other metal is dipped into a solution comprising 1 weight percent of Durad (or equivalent phosphate ester) and 1 weight percent of ferric acetylacetonate in ethanol. The dip is done at room temperature for 1 minute. After the dip, the ethanol is allowed to evaporate, leaving a thin film of the phosphate ester and the ferric acetylacetonate. The substrate is then inserted for 1 minute in an oven that has been preheated to ≈300 °C. This heating causes the formation of a thin film of iron phosphate, as confirmed by x-ray photoelectron spectroscopy.

This work was done by Wilfredo Morales of **Glenn Research Center**.

Inquiries concerning rights for the commercial use of this invention should be addressed to NASA Glenn Research Center, Commercial Technology Office, Attn: Steve Fedor, Mail Stop 4–8, 21000 Brookpark Road, Cleveland, Ohio 44135. Refer to LEW-16680.

Books and Reports

Nanolaminate Mirrors With Integral Figure-Control Actuators

A report discusses the development of thin-shell curved mirrors comprised of metallic multilayer nanolaminate substrates that contain integral in-plane actuators for controlling surface figure with micron-level precision. These mirrors, intended for incorporation into scientific imaging systems, would have areal mass densities of <2 kg/m^2. The development involves the combination of emerging disciplines of nanolayer composite materials, electroactive materials, and mathematical modeling for the understanding and controlling elastic deformations of thin-shell structures. Nanolaminates constitute a relatively new class of materials that can approach theoretical limits of stiffness and strength. For making the proposed mirrors, nanolaminates are synthesized by magnetron sputter deposition of metallic alloys and/or compounds on optically precise master surfaces to obtain an optical-quality reflector. The crystallographic structure of the deposited layers would be controlled to optimize reflector mechanical performance. The report details the mathematical-modeling aspect of the development with a brief discussion of experiments on nanolaminate specimens.

This work was done by Gregory Hickey, Sryh-Shiuh Lih, and Troy Barbee of Caltech for **NASA's Jet Propulsion Laboratory**.

To obtain a copy of the report, "Deformable Thin Shell Nano-Laminate Mirror," see TSP's [page 1].

In accordance with Public Law 96-517, the contractor has elected to retain title to this invention. Inquiries concerning rights for its commercial use should be addressed to

Intellectual Property group
JPL
Mail Stop 202-233
4800 Oak Grove Drive
Pasadena, CA 91109
(818) 354-2240

Refer to NPO-30221, volume and number of this NASA Tech Briefs *issue, and the page number.*

BLANK PAGE

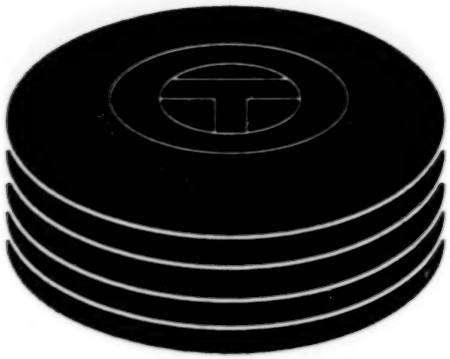

Computer Programs

Electronic Components and Circuits

33 Software for Modeling Spacecraft Electric Power

Electronic Systems

33 Software Implements Telemetry Protocols

Physical Sciences

33 Software for Global Forecasting of Winds and Waves

Mathematics and Information Sciences

33 Program for Tracking Air-Purification Cartridges
34 Software for Implementing Fuzzy Logic on Microcontrollers
34 Software for Constructing a Facility-Management Database
34 Software for Parallel Processing of Telemetry

BLANK PAGE

Electronic Components and Circuits

Software for Modeling Spacecraft Electric Power

Multi-Mission Power Analysis Tool (MMPAT) is a computer program for constructing computational models of the generation, storage, consumption, and flow of electric power in a spacecraft. Heretofore, such modeling has been accomplished by means of unique software for each application. In contrast, MMPAT offers a generic capability for constructing models for diverse applications, thereby potentially reducing development time and cost. MMPAT includes, principally, modeling algorithms and software for a graphical user interface (GUI). The modeling algorithms are encoded in the C programming language because C is commonly used and handles large sets of data fairly well, and because programs written in C can be readily attached to other programs. The GUI software is written Tcl/Tk, which is a scripting language. Tcl/Tk was chosen because it is portable among operating systems, includes a socket interface for connecting to external programs, has the look and feel of a traditional Windows application program, and can be used gratis. Together, the set of algorithms and the GUI software have proven to be a powerful combination that can be compiled into a single executable program.

This program was written by Roy Gladden and Mark Kordon of Caltech for **NASA's Jet Propulsion Laboratory**. *Further information is contained in a TSP [see page 1].*

This software is available for commercial licensing. Please contact Don Hart of the California Institute of Technology at (818) 393-3425. Refer to NPO-30191.

Electronic Systems

Software Implements Telemetry Protocols

The CCSDS Telemetry and Telecom Software Library provides a reference implementation of the Consultative Committee for Space Data Systems (CCSDS) international protocol standard for the transmission and reception of telemetry and telecommand data in radio communications with spacecraft. The library supports the full set of uplink and downlink virtual channels. It includes a frame-acceptance and -reporting mechanism (FARM) that supports a sliding window specified in the CCSDS standard, with routines for specifying the window width. The FARM generates CCSDS-standard command link control words (CLCWs) that indicate the state of the FARM. Routines for incorporating the CLCWs into downlink telemetry streams are included. Test drivers for showing how the library functions within the context of an application program are also included. The library has been written in the C programming language for execution on various computers running the SunOS4, SunOS5, AIX, and VxWorks operating systems. Makefiles that can be tailored for other computers and operating systems are included. Both source code and documentation are provided on the distribution medium, which is a tar file.

This work was done by Steven Allen of Caltech for **NASA's Jet Propulsion Laboratory**. *Further information is contained in a TSP [see page 1].*

This software is available for commercial licensing. Please contact Don Hart of the California Institute of Technology at (818) 393-3425. Refer to NPO-20419.

Physical Sciences

Software for Global Forecasting of Winds and Waves

The WorldWinds™ software system generates high-resolution global weather forecasts, with emphasis on wind and ocean-wave vectors, in nearly real time. WorldWinds™ was developed primarily to serve organizations and individuals needing accurate forecasts for scientific, safety, or economic reasons. WorldWinds™ accepts input data from multiple satellite sources: the TOPEX altimeter, the ERS-2 scatterometer, the QuikScat scatterometer, and the SSM/I microwave radiometer. The software takes those parts of the data that pertain to wind, wave, and other weather observations, combines them with observational data from National Weather Service, and feeds them into two numerical models of weather: the Penn State MM5 model and the Harris Quasi-Lagrangian model. These models generate superior forecasts of wind and wave vectors and other weather variables for periods from 12 to 72 hours. WorldWinds™ is unique in that it can forecast winds over the entire surface of the Earth, producing a seamless global weather map every hour of every day. Data can be given at spatial grid intervals that range from 120 to as little as 3 km. Both spatial and temporal scales can be adjusted to satisfy the needs of clients.

This program was written by Elizabeth L. Valenti and Patrick Fitzpatrick of WorldWinds, Inc., and Samuel W. McCandless, Jr., and Barton Huxtable of User Systems, Inc., for **Stennis Space Center**.

In accordance with Public Law 96-517, the contractor has elected to retain title to this invention. Inquiries concerning rights for its commercial use should be addressed to

WorldWinds, Inc.
John C Stennis Space Center
Bldg 1100, Rm 1125
Stennis Space Center, MS 39529

Refer to SSC-00109, volume and number of this NASA Tech Briefs *issue, and the page number.*

Mathematics and Information Sciences

Program for Tracking Air-Purification Cartridges

The Cartridge Automated Reliance Tracking (CART) computer program enables authorized requesters associated with NASA to gain access to the most recent tracking data on LiOH-based air-purification cartridges used during space-shuttle flights. CART could also be adapted to suit the needs of other organizations in disseminating tracking data to geographically dispersed users. The information provided by CART includes the location and flight status of each cartridge, every step in the processing of the cartridge, and the statuses of all chemicals consumed in the processing. Prior to the development of CART, reports on the statuses of cartridges were prepared manually in Kennedy Space Center's LiOH laboratory on request and transmitted by facsimile — a slow, labor-intensive procedure. CART utilizes Oracle Forms and

Tarantella Web software. Cartridge-tracking data are now stored on a central server computer and made available in a series of reports that are accessible to authorized requesters in real time via the World Wide Web.

This program was written by Christopher L. Ehrenfeld and Stephen M. Schneider of United Space Alliance for **Kennedy Space Center.**

KSC-12179

Software for Implementing Fuzzy Logic on Microcontrollers

Fuzzy Inference System Translator (FIST) is a computer program that facilitates the implementation of fuzzy-logic software on commercial or other viable microcontrollers. In the original application for which FIST was developed, there was a need to implement plant-growth-chamber (PGC) temperature-and-humidity controllers that had been developed within the MATLAB Fuzzy Logic Toolbox software system. In this application, fuzzy membership functions were specified for the temperature and relative-humidity signals, and a set of weighted inference rules was developed from experience and working knowledge of an environmental chamber, containing the PGC, in which the temperature and humidity were to be controlled. First-order models of PGC dynamics, based on the temperature dependences of heat-transfer rates and water-vapor pressure, were used with SIMULINK (mathematical-modeling software compatible with the MATLAB software) for rapid prototyping of a fuzzy inference system. All the information relevant to the controller thus developed are contained in a MATLAB fuzzy-inference-system file. The role of FIST in the development of the present controller or a similar controller is to extract the relevant information from this file and process it into machine code that is executable on a specified microcontroller.

This program was written by Bill Taylor of New Mexico Highlands University for **Kennedy Space Center.** *Further information is contained in a TSP [see page 1].*

In accordance with Public Law 96-517, the contractor has elected to retain title to this invention. Inquiries concerning rights for its commercial use should be addressed to

New Mexico Highlands University
Department of Engineering
National Avenue
Las Vegas, NM 87701

Refer to KSC-12145, volume and number of this NASA Tech Briefs *issue, and the page number.*

Software for Constructing a Facility-Management Database

Facility Management Tracking System (FMTS) is a computer program for constructing an integrated database that defines any event in a managed facility. FMTS provides a simple user interface for entering all relevant data connected to the event. The entered data, as displayed and processed by FMTS, are used by the facility manager to determine the status of the event, control processing steps and to verify other information about the event, approve the control points of the event, and ultimately close out the event. This process assures the requirements for the facility manager's authority over, and accountability for, meeting health and safety in the facility with a certifiable audit trail. The data can then be exported by electronic mail to other database systems maintained by organizations that are responsible for various systems within the facility. FMTS can be executed on standard personal computers and is compatible with commercial off-the-shelf server/client computer systems. The FMTS is designed to integrate modified versions of FMTS into database programs used by a variety of government and commercial organizations that have complex facility-management responsibilities.

This program was written by Thomas E. Diegelman of **Johnson Space Center,** *Jeannie Pullen of Science Applications International Corp., and Charles Shultz and Price Lewis of United Space Alliance. Further information is contained in a TSP [see page 1].*

MSC-23284

Software for Parallel Processing of Telemetry

Parallel Telemetry Processor (PTEP) is a high-speed, robust, extensible, Java-language computer program that (1) enables the parallel processing of a serial stream of telemetric data and (2) generates a graphical display for monitoring the processing. Originally intended for application to spacecraft telemetry, PTEP could also be applied to the processing of data from other complex, heterogeneous systems that generate serial data streams. PTEP provides for multithreaded dispatching of tasks and accommodates the integration of other data-processing application programs into the processing pipeline. The PTEP graphical display is a color-coded flow chart with arrows that indicate the progress of each packet through processing steps. Also represented on the flow chart are intermediate data products and processing steps in which errors occur. Packets that cause processing errors are stored in an error queue for later review while the system continues to process new packets. At any time, a user can obtain detailed information about a processing error, correct the error, and resume processing of the affected packet.

This work was done by Jeffrey Norris, Eric Baumgartner, and Paul Backes of Caltech for **NASA's Jet Propulsion Laboratory.** *Further information is contained in a TSP [see page 1].*

This software is available for commercial licensing. Please contact Don Hart of the California Institute of Technology at (818) 393-3425. Refer to NPO-21223.

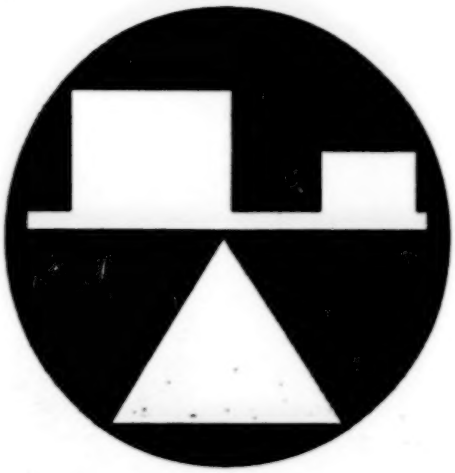

Mechanics

Hardware, Techniques, and Processes

37 Pressure-Balanced, Low-Hysteresis Finger Seal

39 Instrument for Measuring Extreme Winds

Books and Reports

39 Tests of Finger Seals

BLANK PAGE

Pressure-Balanced, Low-Hysteresis Finger Seal

Pressure balance would be altered to reduce a hysteretic variation of leakage.

John H. Glenn Research Center, Cleveland, Ohio

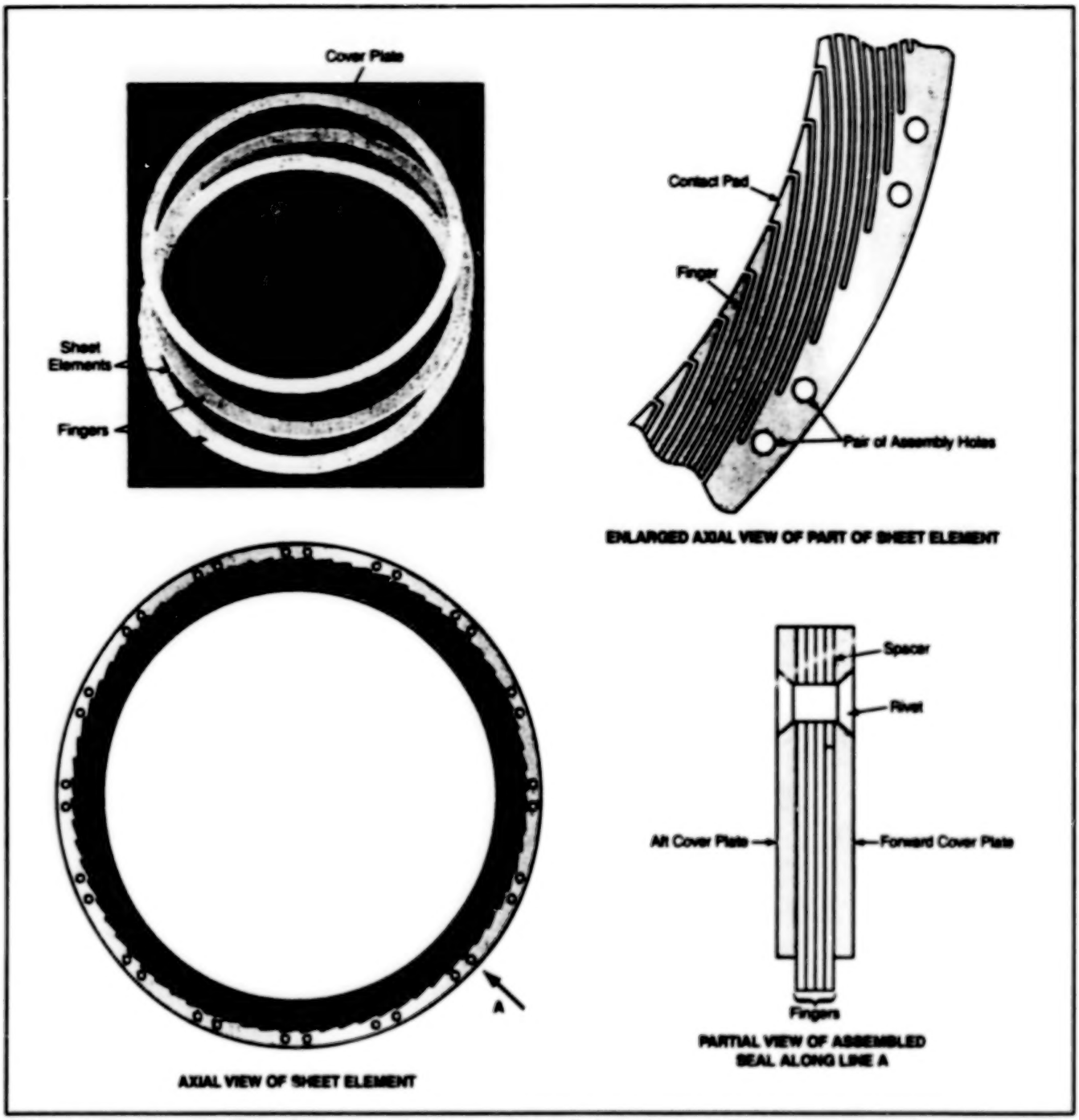

Figure 1. A First-Generation Finger Seal works well at low or monotonically increasing speed, but not during deceleration from high speed.

A second-generation design for a finger seal has been proposed to reduce a hysteretic effect that gives rise to increased leakage in a first-generation finger seal. As explained below, the second-generation design provides for balancing of pressure drops along the flow paths within the seal in such a way as to reduce a friction force believed to cause the hysteresis.

Like a labyrinth or brush seal, a finger seal is used (typically in a gas turbine) to minimize a leakage flow along a rotating shaft. A finger seal partly resembles a brush seal in appearance and function, but costs only about one-fifth as much.

Instead of the random array of fine wires found in a brush seal, a finger seal contains a stack of precisely photoetched sheet elements. The photoetched details of the sheet elements are series of intricate geometrical features repeated at small intervals along the circumference at the inner diameter (see Figure 1.) The key features are slender, curved beams (the fingers) with contact pads at their tips. The fingers spring-load the contact pads into gentle contact with the shaft.

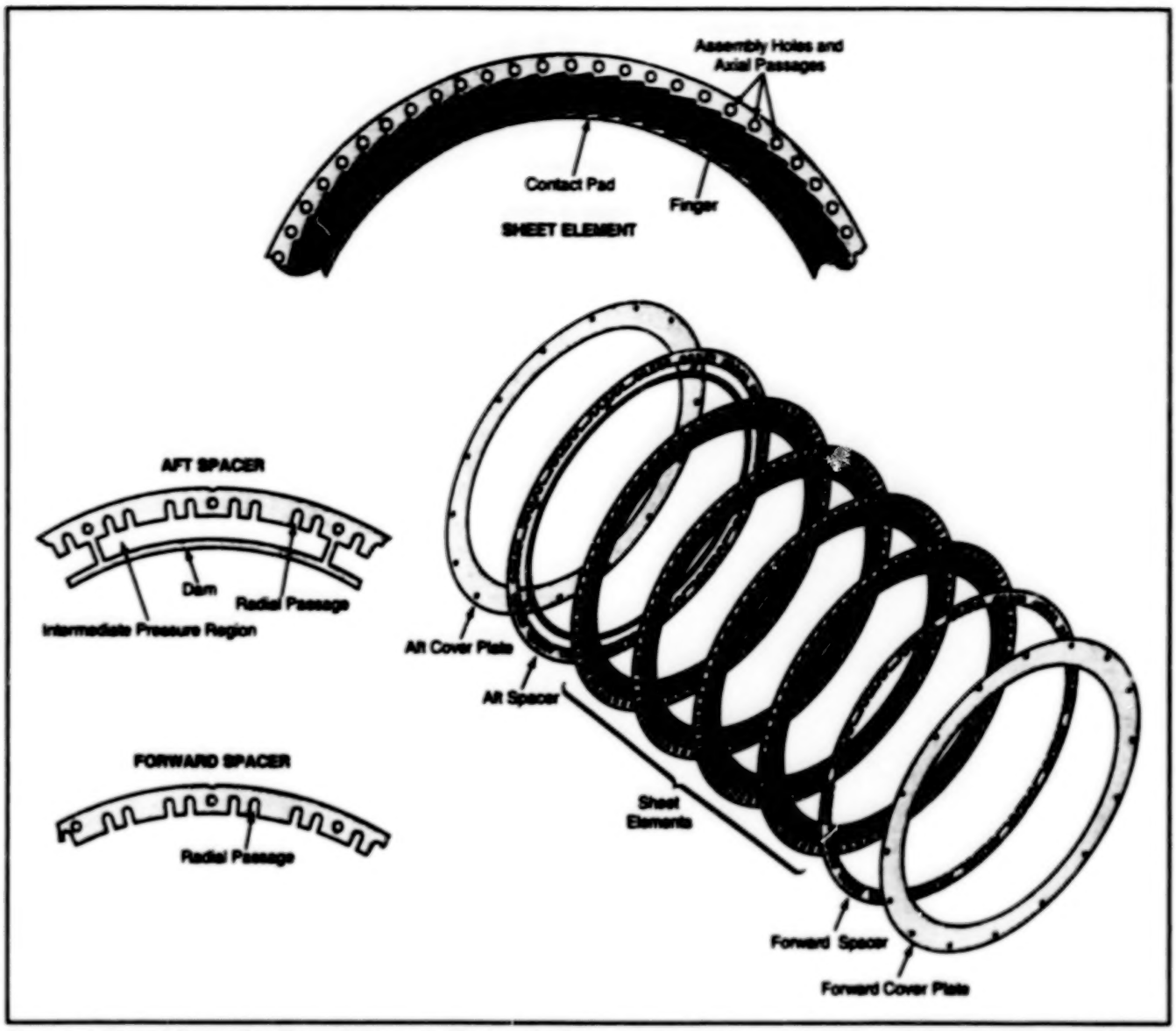

Figure 2. A Second-Generation Finger Seal would differ from the first-generation seal in several details, such that the friction force believed to cause hysteresis would be greatly reduced.

Another key feature is a series of pairs of holes, into which rivets are inserted during assembly of the seal. The holes are spaced such that when successive elements are alternately indexed to the holes, the empty spaces between the finger/pad subelements of each sheet element are covered by finger/pad subelements of the adjacent sheet element. Usually, a first-generation finger seal comprises four sheet elements, a spacer on the forward (high-pressure) side, and forward and aft cover plates.

The seal is fitted over a sealing land on the shaft with a small amount of interference and thus gentle spring loading. Flow through the seal is impeded by the staggered finger/pad features as well as by the radial contact between the land and the pads. The flexible fingers can give radially to accommodate shaft excursions and relative growth of the seal and rotor resulting from rotational forces and thermal expansion.

In tests at constant temperature and pressure, first-generation finger seals exhibited the following hysteretic phenomenon: Leakage remained close to an initial low level as the rotation of the shaft was ramped up from zero to a maximum speed of about 40,000 rpm, but then the leakage increased significantly as the speed was ramped from maximum down to zero. It has been conjectured that (1) as the speed increases, the fingers move out in response to a combination of centrifugal growth of the rotor, thermal mismatch, rotor runout, and other causes; and (2) as the speed decreases, the seal fingers do not spring back and instead become stuck in their radially outermost positions, so that the seal/shaft gaps become wider, allowing more leakage. It has been further conjectured that the reason the fingers become stuck in their outermost positions is that the force of friction between the aft cover plate and the fingers is greater than restoring spring force of the fingers.

The proposed second-generation design would reduce the pressure-drop force between the aft cover plate and the adjacent finger/pad subelements, thereby reducing the friction force believed to cause the hysteresis. A second-generation finger seal (see Figure 2) would comprise forward and aft cover plates, forward and aft spacers, and four sheet elements. By means of a series of radial and axial passages, the gap between the forward plate and the foremost sheet element would be connected to the gap between the aft cover plate and the aftmost sheet element. This connection would cause the intermediate pressure between the aft cover plate and the aftmost sheet element to track very closely

the high pressure at the forward end. The aft cover plate would include a narrow dam in contact with the finger subelements of the aftmost sheet element. This dam would provide the seal between the intermediate pressure and the low pressure.

This work was done by Gulshan K. Arora and Donald L. Glick of Allied-Signal Aerospace Co. for **Glenn Research Center**. *Further information is contained in a TSP [see page 1].*

Inquiries concerning rights for the commercial use of this invention should be addressed to NASA Glenn Research Center, Commercial Technology Office, Attn: Steve Fedor, Mail Stop 4–8, 21000 Brookpark Road, Cleveland, Ohio 44135. Refer to LEW-16840.

Instrument for Measuring Extreme Winds

This rugged instrument has no moving parts.

John F. Kennedy Space Center, Florida

An instrument is undergoing development for use in measuring both the horizontal direction and the horizontal speed of wind in the speed range from 60 to 300 mph (about 27 to 134 m/s) at a rate of at least 50 samples per second. The speed range of this instrument greatly exceeds that of conventional anemometers, encompassing speeds observed in hurricanes and tornadoes. Unlike conventional anemometers, this instrument has a small exposure profile and contains no rotating mechanisms and, hence, is more rugged.

This instrument is based on measurement of the force exerted by wind on a stationary vertical rod. For the purpose of obtaining readings proportional to the wind force in two orthogonal horizontal directions, one end of the rod is attached to a cruciform carrier plate, the orthogonal arms of which are instrumented with strain gauges (see figure). The aerodynamic load on the rod causes the crossed arms to bend somewhat, and the bending is measured by the strain gauges.

The aerodynamic force on a rod in a cross flow is well understood and is a function of the Reynolds number. The force includes a steady component proportional to drag, which, in turn, is proportional to the square of the wind speed. In addition, over a certain range of the Reynolds number, vortices are periodically shed from the rod, giving rise to a side-to-side oscillating force, the frequency of which is linearly proportional to the wind speed. Hence, the strain-gauge outputs include steady drag components and oscillatory vortex-shedding components that are related to the wind velocity in known ways.

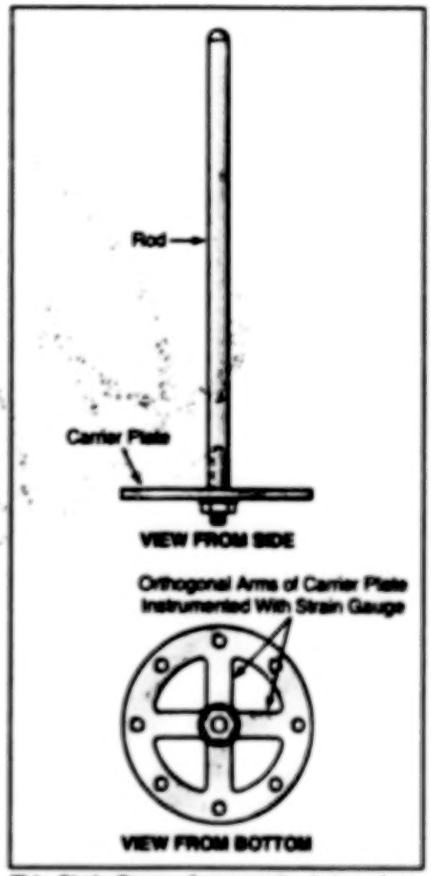

This **Strain-Gauge Anemometer** is based on strain-gauge measurement of bending in the orthogonal arms of the carrier plate. The bending is related in a known way to the wind load on the rod.

A signal-processing technique has been devised to extract, from the steady and oscillatory components of the strain-gauge outputs, two independent indications of the wind speed. These two indications can then be used to obtain an optimal estimate of the wind speed. When fully developed, the instrument will also include signal-processing electronic circuitry and data-storage circuitry. An internal battery power supply is an important element of the design inasmuch as commercial power would be unreliable in a major storm and should possibly make the instrument more vulnerable to damage by lightning.

This work was done by Jan Zysko of **Kennedy Space Center** *and Stan Starr of I-NET, Inc. Further information is contained in a TSP [see page 1].*

KSC-11886

Books and Reports

Tests of Finger Seals

A report discusses tests of finger seals, which were described in "Pressure-Balanced, Low-Hysteresis Finger Seal" (LEW-16840), *NASA Tech Briefs*, this issue, page 37. Like a labyrinth or brush seal, a finger seal is used (typically in a gas turbine) to minimize a leakage flow along a rotating shaft. A finger seal contains a stack of sheet elements that have been precisely photoetched into a series of slender, curved beams (the fingers) with contact pads at their tips, located at small intervals along the circumference at the interface with the shaft. The fingers spring-load the contact pads into gentle contact with the shaft. The report describes baseline (subject to considerable hysteresis) and pressure-balanced (low-hysteresis) brush seals and presents results of hysteresis, performance, and endurance tests of the seals in a seal rig at Glenn Research Center. The report concludes that a finger-seal design is ready for engine testing.

This work was done by Margaret P. Proctor and Bruce M. Steinetz of **Glenn Research Center**, *Gul K. Arora of AlliedSignal Engines, and Irebert R. Delgado of the U. S. Army Research Laboratory. To obtain a copy of the report, "Pressure-Balanced, Low-Hysteresis Finger Seal Test Results" see TSP's [page 1].*

Inquiries concerning rights for the commercial use of this invention should be addressed to NASA Glenn Research Center, Commercial Technology Office, Attn: Steve Fedor, Mail Stop 4–8, 21000 Brookpark Road, Cleveland, Ohio 44135. Refer to LEW-16973.

BLANK PAGE

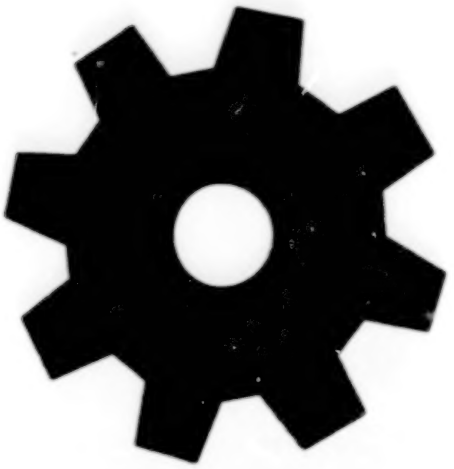

Machinery

Hardware, Techniques, and Processes

43 Emergency Landing Using Thrust Control and Shift of Weight

44 Mechanized Harvesting of Plants in a Controlled Environment

BLANK PAGE

Emergency Landing Using Thrust Control and Shift of Weight

Landing with control surfaces and engines on one side inoperative may be possible.

Dryden Flight Research Center, Edwards, California

Normally, the damage that results in a total loss of the primary flight control of a transport airplane, including all the engines on one side, would be catastrophic. Dryden Flight Research Center has conceived of a method of responding to a total loss of hydraulic pressure and failure of engines on one side: An emergency controller would utilize the engines that are still working on the other side, along with transfers of fuel among tanks to effect lateral shift of the center of gravity (CG), in order to steer the airplane to an emergency landing.

Many occurrences have made it necessary to use engine thrust to supplement or even replace the normal flight controls of aircraft. Most of these occurrences have resulted in crashes, in which a total of more than 1,200 lives have been lost (see "Throttles Land Disabled Jet" by Michael Dornheim, Aviation Week & Space Technology, September 4, 1995, pages 26 and 27).

Dryden Flight Research Center has developed a propulsion-controlled aircraft (PCA) system, in which computer-controlled thrust provides an emergency control capability without using any of the normal control surfaces. Using a PCA system, an F-15 and an MD-11 airplane have landed without using any moving control surfaces. In all the cases studied, the thrust of the engines on both sides of the airplane was available. Figure 1 shows the first MD-11 PCA landing accomplished by use of thrust modulation with all the engines working and no moving control surfaces.

Consider an airplane on which a bomb blast has disabled the hydraulics (making the control surfaces inoperative) as well as the engine or engines on one side. Could an emergency controller be designed to land the airplane? A preliminary investigation has shown that one wing engine can be operated to obtain limited flight control if the lateral center of gravity (CG-Y) is shifted toward the wing with the working engine. Simulations of the MD-11 with all conventional flight controls inoperative and a wing engine inoperative have shown positive control capability within the available range of CG-Y offset. Simulations of such four-engine airplanes as the B-720 and B-747, have also shown positive control capability within the available ranges of CG-Y offsets.

U.S. Patent 6,126,111 documents this emergency controller. On large commercial airplanes, engines are usually located under both wings, either singly or in pairs, and

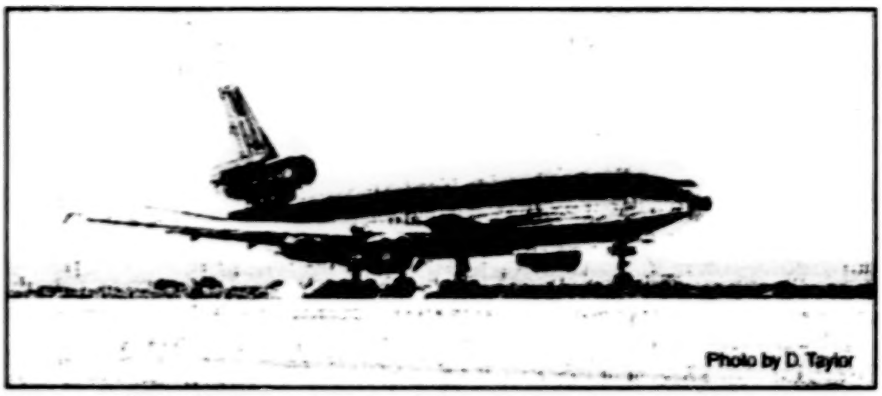

Figure 1: An MD-11 Airplane is shown here landing with thrust control only (that is, with control surfaces not moving).

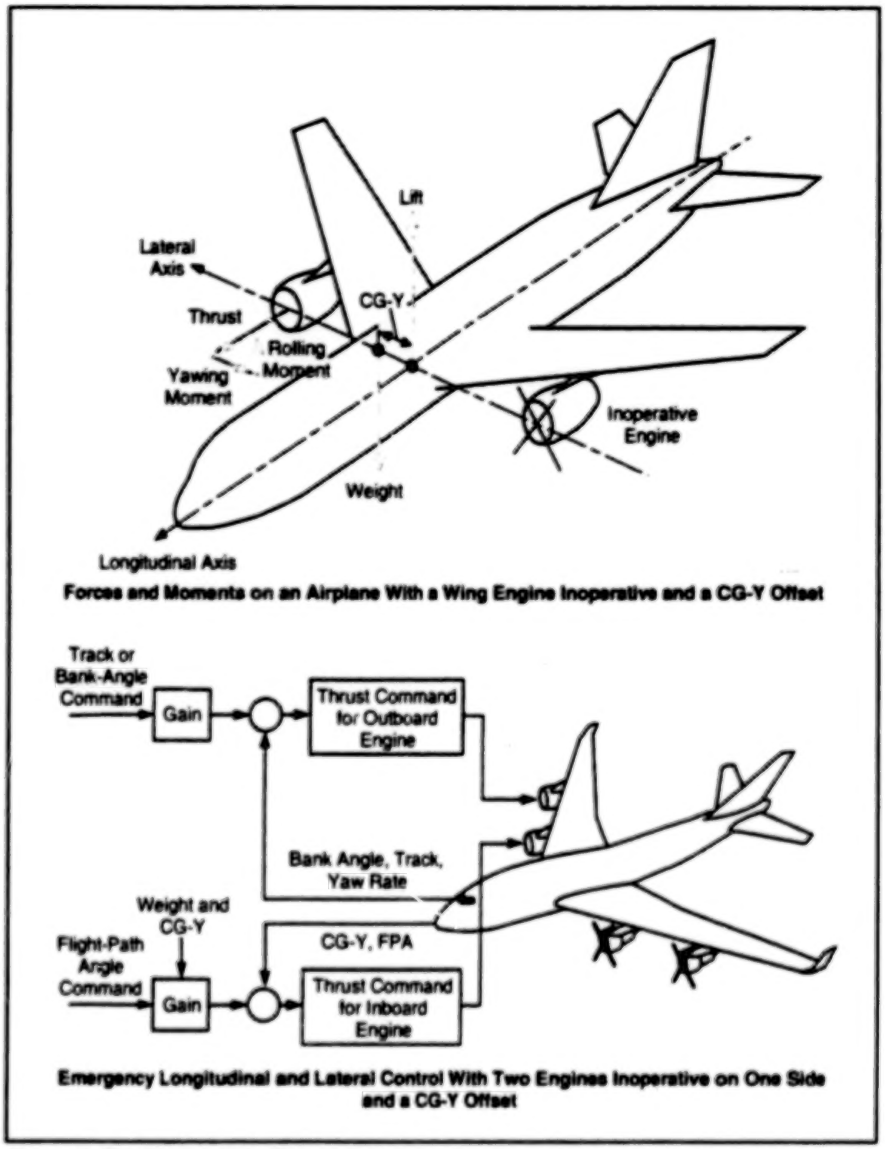

Figure 2. The Asymmetric Forces that arise when the engines on one side and the control surfaces are inoperative are countered by use of an emergency controller, which varies the thrust of the working engines and transfers fuel among tanks to shift the center of gravity toward the working-engine side.

large amounts of fuel are carried for long journeys. The fuel tanks are distributed throughout the wings and cargo sections of the airplanes. The transfer of fuel among the tanks of an airplane to shift its CG-Y is a well known and frequent practice.

Fuel can be transferred selectably and independently among all fuel tanks. On the MD-11 airplane, each wing tank holds 42,000 lb (≈19,000 kg) of fuel and the maximum CG-Y shift observed in tests was 45 in. (1.14 m) in 15 minutes, corresponding to an average rate of change of CG-Y of about 3 in. (≈7.6 cm) per minute. On the B-747 airplane the wing fuel capacity is 84,000 lb (≈38,000 kg) in each inboard tank and 30,000 lb (≈13,600 kg) in each outboard tank, and the maximum CG-Y shift observed was 70 in. (1.78 m).

The upper part of Figure 2 illustrates the case of an airplane with inoperative control surfaces and only one operating engine. The CG-Y is shifted toward the side with the working engine. The thrust of the operating engine creates yawing and rolling moments to counter the rolling moment resulting from the drag of the nonoperating engine. The lower part of Figure 2 depicts the emergency-control scheme. The results of simulations of the use of this control scheme on the MD-11 and B-747 have shown that level flight can be maintained. Increasing thrust rolls the airplane away from side of the working engine. Roll rates of 5°/s are typical. This control scheme makes it possible to align the airplane with the center line of a runway and, most likely, to have a survivable landing. Of course, practice landings in a simulator or during a high-altitude flight above a real runway are needed to increase the likelihood of a survivable landing.

This work was done by John J. Burken, Bill Burcham, and Jeanette Le of **Dryden Flight Research Center**.

This invention has been patented by NASA (U.S. Patent No. 6,126,111). Inquiries concerning nonexclusive or exclusive license for its commercial development should be addressed the Patent Counsel, Dryden Flight Research Center [see page 1]. Refer to DRC-96-55.

Mechanized Harvesting of Plants in a Controlled Environment

The proposed Plant Harvesting Mechanization System (PHARMS) would comprise machinery and controls for semiautomated harvesting of plants grown in a controlled environment. The PHARMS was conceived as a prototype of harvesters to be incorporated into life-support systems of spacecraft and remote planetary bases, wherein plants would provide food and contribute to recycling of air and water. On Earth, PHARMS-like systems could reduce the labor of harvesting plants from protected agricultural systems in which special fruits and vegetables, herbs, ornamental plants, and mushrooms are grown. At harvest time, the PHARMS would be moved from storage to a location near the plant-growth chamber. There, it would be unfolded from a compact configuration, then prepared for operation by setting of control parameters and mechanical alignment with the chamber and plants. In operation, the PHARMS would pull plant trays out of the chamber and remove plants from the trays. Then it would subject the plants to a variety of other processes, depending on the crop: Examples of such processes include drying, cutting, chopping, stripping of seeds from stalks, threshing, separation of roots from stalks or vines, breaking pods to extract seeds, and pneumatic separation of seeds from chaff.

This work was done by Jeffrey T. Iverson, Chad Ehle, Andrea Hill, and Robert Birnschein of Orbital Technologies Corp. for **Kennedy Space Center**.

In accordance with Public Law 96-517, the contractor has elected to retain title to this invention. Inquiries concerning rights for its commercial use should be addressed to

Thomas M. Crabb
Orbital Technologies Corp.
1212 Fourier Drive
Madison, WI 53717
Tel No.: (608) 827-5000
E-mail: crabbt@orbitec.com

Refer to KSC-12143, volume and number of this NASA Tech Briefs *issue, and the page number.*

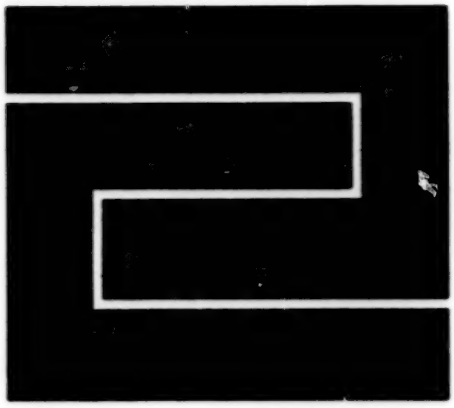

Fabrication Technology

Hardware, Techniques, and Processes

47 High-Velocity, Pulsed Wire Arc Spray

BLANK PAGE

High-Velocity, Pulsed Wire Arc Spray

Higher spray velocity should result in superior deposits.

Marshall Space Flight Center, Alabama

A high-velocity, pulsed wire arc spraying apparatus has been proposed and partly developed in an effort to improve the quality of coatings deposited by thermal spray techniques. In this apparatus, material from a wire arc is atomized and propelled toward a deposition substrate by a repetitively pulsed plasma jet. As explained below, this development is prompted by (1) the observation that the particle velocities attainable in traditional wire arc spraying are too low to enable the deposition of dense, high-quality coating materials that are often desired and (2) the expectation that higher spray velocities should result in superior coatings.

In traditional wire arc spraying, an arc is drawn between the proximate tips of two insulated metallic wires and the wires are continuously fed toward the arc as the arc consumes them. (Sometimes one of the wires is replaced by a nonconsumable electrode.) A steady stream of gas (usually compressed air) is directed through the arc to atomize the molten wire material in the arc and propel the resulting droplets toward a deposition substrate. One principal disadvantage of the conventional wire arc spray technique has been the low particle velocity obtained, generally limited to ≈ 250 m/s as a consequence of the fundamental physical nature of the steady gas stream. It is desirable to increase the velocity in order to minimize droplet cooling in the cold gas stream, to eliminate in-flight oxidation of the droplets, and to produce zero porosity coatings.

The UTRON Pulsed Wire Arc Spray device integrates the excellent accelerating characteristics of pulsed plasmas with the simplicity of wire arc systems. The basic approach is to replace the compressed gas stream used in conventional wire arc spray with a repetitive, high-pressure, high-momentum flux pulsed plasma jet. The plasma jet is generated by a so-called capillary arc discharge in a gas or liquid located between electrodes at each end of a long narrow ceramic tube. It is called a capillary discharge due to the high length/diameter ratio, typically about 10 or so. The high-speed plasma jet exiting from a nozzle at the one open end of the capillary is oriented to aim the jet through the arc between the wire tips.

The plasma jet can be formed from a wide range of working fluids, but the work to date has utilized either cryogenic liquid argon or gaseous argon. Liquid argon can be injected as a thin stream into the capillary region either continuously or through fast-acting valves or check valves. The injection orifice, located at the rear end of the capillary, is sized to admit a quantity of liquid equivalent to room-temperature gas at up to 30 atm (~3 MPa). A high-voltage spark discharge triggers electrical breakdown through the gas or vaporizing liquid, which then triggers the main arc discharge along the length of the capillary. Highest performance is achieved with liquid injection since that introduces sufficient mass of gas to attain high pressure without exceeding temperature limits of the ceramic wall. The pulsed discharge quickly raises the pressure and temperature of the working fluid in the capillary to about 1 kbar (100 MPa) and 1 eV (11,600 K), resulting in a high-velocity jet exiting through the nozzle at the end of the tube.

The coating-material wires are positioned through holes in the expansion nozzle attached to the front end of the capillary tube. The arc discharge between the wires can occur either a few microseconds before or after initiation of the plasma jet discharge. In the latter case, the plasma jet itself provides a convenient breakdown path for the wire arc.

The pulsed plasma jet strips the molten metal from the wire tips, atomizes the droplets, and rapidly accelerates the resulting atomized metal droplets to speeds comparable to the plasma. These droplets are then deposited on a substrate or other piece of equipment. The entire process lasts about 100 to 250 μs and can be repeated hundreds of times per second.

The effectiveness of the pulsed wire arc spray device in atomizing and accelerating droplets derives from the extremely high momentum flux (ρv^2) of the pulsed plasma jet. The high-momentum flux is achieved mainly by an order of magnitude increase in velocity v, but also by a similar increase in density ρ when liquid injection is utilized.

To date, the Pulsed Wire Arc Spray device has been operated at single pulse energies up to 4.2 kJ with liquid argon, and at repetition rates as high as 20 Hz at lower energy. Deposition rates as high as 2 kg/h were demonstrated, limited only by the available power supply. Experimental measurements established droplet velocities of up to nearly 1,500 m/s in acceleration distances as short as 3.2 cm, thus making this an ideal process for spraying the inner walls of confined regions (such as cylinder bores and pipes) where space is limited.

This work was performed by F. Douglas Witherspoon, Russell W. Kincaid, and Dennis Massey of UTRON Inc. for **Marshall Space Flight Center.** *UTRON has been awarded U.S. Patent 6,001,425 for this pulsed high-velocity wire arc spraying device. For further information about the current status of this invention, please contact Dr. Russell Kincaid or Dr. Douglas Witherspoon at UTRON at (703) 369-5552 or by e-mail at rwkincaid@erols.com. See also web page at www.utroninc.com.*

Inquiries concerning rights for the commercial use of this invention should be addressed to the Patent Counsel, Marshall Space Flight Center [see page 1]. Refer to MFS-31491.

BLANK PAGE

Mathematics and Information Sciences

Hardware, Techniques, and Processes

51 Massively Parallel Computation of Electromagnetic Fields
51 Physical Model of Immune-Inspired Computing
52 Mathematical Model of a Quantum Decision Maker
52 IIR Filters for Postprocessing Noisy Test Data

BLANK PAGE

Massively Parallel Computation of Electromagnetic Fields

Maxwell's equations are solved by fully implicit finite-difference techniques.

NASA's Jet Propulsion Laboratory, Pasadena, California

A method of massively parallel computation on supercomputers has been developed to facilitate numerical simulation of electromagnetic fields in the vicinities of electrically large and complex radiating and scattering objects. In this method as in methods developed previously for the same purpose, Maxwell's equations are solved by use of finite-difference approximations in both space and time. However, unlike in the other methods, this method is not limited to implicit (and thus parallel) solution in space with explicit (and thus sequential) time stepping with small time steps to ensure numerical stability. Instead, this method provides for parallel solution for all time steps, and the time steps can be larger and thus fewer — this characteristic is often characterized in the literature as "coarse-grained parallelism."

This method follows an approach that combines the fully implicit Crank-Nicolson time-stepping method with a massive degree of parallelism in computation. This approach enables the application of fully implicit techniques; in comparison with explicit techniques, implicit techniques exhibit superior numerical properties (principally, unconditional stability) while also providing optimal efficiency for parallel computation. The time-parallel algorithm in this method imposes relatively simple requirements for communication and synchronization among different processors; this characteristic in combination with coarse-grained parallelism, makes for highly efficient implementation on emerging massively parallel multiple-instruction, multiple-data computers.

The basic equation of the method is obtained by applying the Crank-Nicolson method to the second-order inhomogeneous

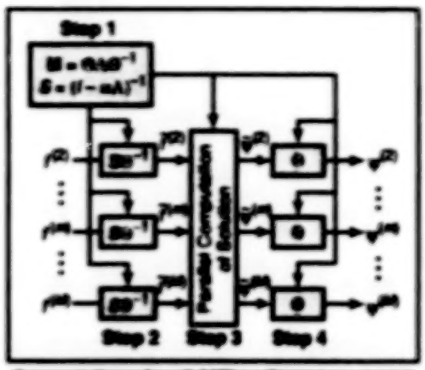

Computations for all *M* Time Steps in a numerical simulation of a spatially complex, time-dependent electromagnetic field are performed in parallel.

linear recursion (SOILR) equation of the finite-difference formulation of the Maxwell's equations. The resulting form of the basic equation is

$$(I - \alpha\mathbb{M})\psi^{(m+1)} = 2I\psi^{(m)} - (I - \alpha\mathbb{M})\psi^{(m-1)} + f^{(m+1)} \text{ for } 1 < m < M - 1,$$

where I is the identity matrix, α is a constant, $\mathbb{M}$ is an $N \times N$ matrix that arises from the spatial discretization of the Laplacian operator in Maxwell's equations, $\psi^{(m)}$ denotes the solution (a vector that represents the electromagnetic-field quantity of interest) at the mth time step, and $f^{(m)}$ denotes the time- and space-discretized source term for initial and boundary conditions at the mth time step. The eigenvalue/eigenvector decomposition of $\mathbb{M}$ is given by $\mathbb{M} = \Theta\Lambda\Theta^{-1}$, where Θ is the set of eigenvectors and Λ is a diagonal matrix that represents the set of eigenvalues of $\mathbb{M}$.

Let there be a diagonal matrix

$$S = (I - \alpha\Lambda)^{-1}.$$

Let

$$\tilde{\psi}^{(m)} = \Theta^{-1}\psi^{(m)} \text{ and } \tilde{f}^{(m)} = S\Theta^{-1}f^{(m)}.$$

Then it can be shown that the basic equation can be put in the form

$$\tilde{\psi}^{(m+1)} = 2S\tilde{\psi}^{(m)} - \tilde{\psi}^{(m-1)} + \tilde{f}^{(m+1)}.$$

Unlike the basic SOILR equation as formulated in the preceding paragraph, this SOILR equation is diagonalized and can therefore be solved efficiently by use of either of two parallel-computation algorithms called the Recursive Doubling Algorithm (RDA) or the Cyclic Reduction Algorithm (CRA). For two- and three-dimensional problems, this SOILR equation can be solved in $O(N^2 \log M)$ and $O(N^3 \log M)$, respectively, on M processors, where $O(x)$ denotes an amount of computing time or a number of arithmetic operations proportional to a number of the order of x.

The figure illustrates the time-parallel algorithm, which is divided into four steps. Step 1 involves determination of the eigenvalue/eigenvector decomposition of $\mathbb{M}$ and the computation of S. In step 2, the source vectors $f^{(m)}$ are computed and multiplied by $S\Theta^{-1}$ to obtain $\tilde{f}^{(m)}$. The parallel computation to solve the diagonalized form of the basic SOILR equation is performed in step 3, yielding the vectors $\tilde{\psi}^{(m)}$. The desired solution vectors are computed in step 4 by matrix-vector multiplication; namely,

$$\psi^{(m)} = \Theta\tilde{\psi}^{(m)}.$$

This work was done by Amir Fijany, Michael A. Jensen, Yahya Rahmat-Samii, and Jacob Barhen of Caltech for **NASA's Jet Propulsion Laboratory**. *Further information is contained in a TSP [see page 1].*
NPO-19453

Physical Model of Immune-Inspired Computing

This model simulates several basic cellular and global functions of immune systems.

NASA's Jet Propulsion Laboratory, Pasadena, California

A mathematical model that represents several physical and mental behaviors has been developed to enable the phenomenological description of basic functions of immune systems. This development is part of a continuing effort to improve the autonomy of robots and spacecraft by use of computational methods that exploit paradigms of human immune systems. The model can serve as a formalism for building artificial immune systems for computing and for other forms of information processing.

The discipline of artificial immune systems is a rapidly growing field of information processing based upon immune-inspired paradigms of nonlinear dynamics. The interest in immune-systems paradigms stems from the observation that an immune system serves as an excellent model of adaptive processes that occur at the local (cellular) and of useful behavior emerging at the global level.

Although artificial immune systems have many features in common with artificial neural networks, there are some differences that arise from the fact that immune systems perform many different functions simultaneously and, in comparison with neural networks, they are more complex and more diverse. In contradistinction to a neural network, an immune system, from the perspective of nonlinear dynamics, can

be considered as a multibody system (the bodies being cells) in which the bodies are interconnected via flows of information. Inasmuch as these flows and the responses to them may be distorted, delayed, or incomplete, the motion of each cell becomes stochastic and can be simulated as a controlled random walk.

One of the main challenges in modeling living systems is to distinguish random walks of physical origin (for instance, Brownian motions) from those of biological origin. Following a line of reasoning from prior research, it was assumed, in the development of the present model, that a biological random walk must be nonlinear. The model is intended, more specifically, to simulate the main immune-system functions based on the dynamics of body cells interacting with invader cells. In contradistinction to prior stochastic models, the present model incorporates the concept of reflection; that is, the human ability to observe one's own thoughts. This concept renders the model more adaptable to the world of biological and social evolutionary processes.

The model consists of (1) a generator of stochastic processes that represents motor dynamics in the form of nonlinear random walks and (2) a simulator of the nonlinear version of the Fokker-Planck equation, representing the mental dynamics. Thus, the model is one of coupled mental/motor dynamics incorporating the concept of self-image. It has been demonstrated that the model can simulate such basic functions of immune systems (and of cells within immune systems) as self-identification, self/nonself discrimination, self-repair, formation of acquired immunity, self-organization, predator/prey pursuit, and reproduction.

This work was done by Michail Zak of Caltech for **NASA's Jet Propulsion Laboratory**. *Further information is contained in a TSP [see page 1].*
NPO-21039

Mathematical Model of a Quantum Decision Maker

Autonomy would be achieved by use of feedback from mental to motor dynamics.

NASA's Jet Propulsion Laboratory, Pasadena, California

A mathematical model of a quantum analog-computing device that would simulate the human decision-making process has been developed. Like the immune-inspired-computing model described in the preceding article, this model is intended to contribute to improvement in the autonomy of robots and spacecraft.

The device would include quantum recurrent networks that would represent motor dynamics, plus classical neural networks that would represent the evolution of probabilities of processes that, in turn, would represent mental dynamics. The decision-making process would be made autonomous by use of feedback from mental to motor dynamics. In the model, this feedback changes a stochastic matrix based upon distributions of the probabilities. The resulting coupled motor and mental dynamics are described by nonlinear Markov chains that can decrease entropy without recourse to an external source of information.

In terms of mental phenomena, the feedback would play the role of "common sense" in the form of invariants or patterns of behavior that can be abstracted from prior knowledge and experience and can be applied to whole classes of situations similar to those of immediate interest. Like "common sense," this feedback would be used in the quantum decision maker to replace unavailable external information by information from an internal knowledge base. The human ability to do this is recognized and widely exploited in psychology and has been known, since the time of ancient philosophers, to follow from the fact that a human possesses a self-image and interacts with it.

In the model, a quantum recurrent network is regarded as a quantum system represented by an equation that describes the relationships among (1) the inputs to the network at time t, (2) the outputs of the network at a later time $t + \tau$, (3) a set of unitary operators that are defined by the Hamiltonian operator of the quantum system and express the temporal evolution of the quantum system, and (4) a measurement operator that projects the evolved quantum state into one of the eigenvectors of the system. The effect of the measurement operator can be characterized as similar to that of a sigmoid function in a classical neural networks. Because of the stochastic nature of quantum measurements, the outputs at time $t + \tau$ are random; as such, these outputs form a Markovian stochastic process.

The internal knowledge base is stored in a mental submodel in the form of probability distributions. Formally, the knowledge base is represented by the synaptic weights of neural networks, and the knowledge is divided into two parts. The first part includes knowledge that pertains to personal experience, habits, and such inclinations as averseness or proneness to risk. The second part depends upon an objective formulated in terms of probability invariants. Dependence upon the objective can include learning modeled by real-time adjustment of synaptic weights, adapted from theory of neural networks. As soon as the synaptic weights are determined, the common-sense-simulator portion of the model follows an optimal strategy, regardless of unexpected changes in the external world.

This work was done by Michail Zak of Caltech for **NASA's Jet Propulsion Laboratory**. *Further information is contained in a TSP [see page 1].*
NPO-21038

IIR Filters for Postprocessing Noisy Test Data

A little-known parametric form of an infinite impulse response (IIR) filter has been found to be useful in digital postprocessing of noisy test signals. The filter equation is:

$$y(n) = \alpha[x(n) + x(n-1)] + \gamma y(n-1),$$

where α and γ are parameters and $x(n)$ and $y(n)$ are the input and output, respectively, during the nth sampling period. The parameters are given by

$\gamma = \cos\theta_c/(1 + \sin\theta_c)$ and $\alpha = (1 - \gamma)/2$, where $\theta = 2\pi f/f_s$; $\theta_c = 2\pi f_c/f_s$; and f, f_s, and f_c are frequencies. This parametric form simplifies postprocessing and analysis of the data by making it easy to tune the filter response through selection of the low-pass cutoff frequency, f_c. Whereas parameters in other forms of IIR filters are restricted to discrete values, the parameters in this form can be selected from nearly continuous ranges. The filter response in this form is inherently stable over the entire digital frequency range from zero to the Nyquist frequency (half of the sampling frequency, f_s). Although the stability is robust, it deteriorates with a decrease in the number of bits used to represent coefficients and filter states.

This work was done by Jan A. Zysko and Christopher M. Arris of **Kennedy Space Center** *and John E. Lane of Dynacs, Inc. Further information is contained in a TSP [see page 1].*
KSC-12218

END

09-10-02